

Host Spatial Heterogeneity and the Spread of Vector-Borne Infection

Thomas Caraco, Maria C. Duryea, and Stephan Glavanakov

Department of Biological Sciences, University at Albany, Albany, New York 12222

and

William Maniatty¹ and Boleslaw K. Szymanski

Department of Computer Science, Rensselaer Polytechnic Institute, Troy, New York 14810

Received October 23, 1999

We analyze how spatial heterogeneity in host density affects the advance of vector-borne disease. Infection requires vector infestation. The vector spreads only between hosts occupying the same neighborhood, and the number of hosts varies randomly among neighborhoods. Simulation of a spatially detailed model shows that increasing heterogeneity in host abundance reduces pathogen prevalence. Clumping of hosts can limit the advance of the vector, which inhibits the spread of infection indirectly. Clumping can also increase the chance that the pathogen and vector become physically separated during the initial phase of the epidemic process. The latter limitation on the pathogen's spread, in our simulations, is restricted to small interaction neighborhoods. A mean-field model, which does not maintain spatial correlations between sites, approximates simulation results when hosts are arrayed uniformly, but overestimates infection prevalence when hosts are aggregated. A pair approximation, which includes some of the simulation model's spatial correlations, better describes the vector infestation frequencies across host spatial dispersions. © 2001 Academic Press

1. INTRODUCTION

Many epidemic processes, especially those affecting plant populations, may be governed by spatial variation in host abundance (Burdon and Chilvers, 1975; Swinton and Anderson, 1995; Real and McElhany, 1996; Bolker, 1999). Localized contacts between susceptible and infectious individuals, or between susceptibles and disease vectors, commonly drive the advance of disease (Dwyer, 1992). Heterogeneity in host density can induce variation in the number of susceptibles contacted, and so influence the chance that a disease advances when rare (Keeling and Grenfell, 1997; Caraco *et al.*, 1998) and the frequency

of infection when an epidemic occurs (Duryea *et al.*, 1999).

This paper analyzes effects of host spatial heterogeneity on disease spread by a biological vector (Szymanski and Caraco, 1994; McElhany *et al.*, 1995). We find that increased spatial variation in the local density of host individuals decreases the proportion of the host population infected during an epidemic. Host spatial heterogeneity may impede the advance of the vector, and so constrain the spread of infection, or may increase the chance that a pathogen becomes spatially separated from its advancing vector.

1.1. Spatial Heterogeneity and Epidemic Models

Lattice-based epidemic models usually assume that no more than one host individual can occupy any single

¹ Present address: Department of Computer Science, University at Albany, Albany, New York 12222.

location and that a pathogen advances through direct transmission from infectious to susceptible hosts (Durrett and Levin, 1994; Rhodes and Anderson, 1996). A distinguishing property of these models is that the probability that a susceptible host acquires the pathogen depends on the local density of infectious hosts, rather than their global density (e.g., Mollison and Kuulasmaa, 1985; Szymanski and Caraco, 1994; Holmes, 1997).

Many natural populations exhibit significant variation in local density (Greig-Smith, 1979; Burdon *et al.*, 1989). If this heterogeneity scales at distances over which a pathogen is transmitted between hosts, different infectives will interact with different numbers of susceptibles. Infection transmission probabilities will consequently vary spatially in a manner depending on both local host density and local infection frequency (Onstad *et al.*, 1990).

We previously analyzed effects of host spatial heterogeneity on lattice-based epidemics with direct infection transmission (Caraco *et al.*, 1998; Duryea *et al.*, 1999). We considered a spatial epidemic with recovery (Bramson *et al.*, 1989). Host population size was held constant. A susceptible could acquire a pathogen only from a nearby infectious host. Once infected, a host could recover without immunity. Caraco *et al.* (1998) studied the pathogen's probability of rapid extinction and found that increasing host spatial aggregation decreases the probability that the disease advances when rare. For a given global host density, greater spatial heterogeneity increases the number and size of "gaps" in the host population (see Neuhauser, 1998). The gaps inhibit diffusive coupling of infection between hosts or clumps of hosts (Gerhardt *et al.*, 1990). The resulting increase in the probability that an infectious host fails to transmit the pathogen before recovery increases the chance of pathogen extinction. See Bolker (1999) for analysis of a similar process.

If the pathogen avoids rapid extinction (see Durrett and Levin, 1994; Rand *et al.*, 1995), infection and recovery processes may equilibrate at some spatial scale, producing an endemic level of infection. Duryea *et al.* (1999) modeled endemic levels of directly transmitted infection; both analytical and simulation results indicated that greater host spatial heterogeneity reduces endemic infection frequencies.

This paper analyzes disease spread by a biological vector. After sketching an example motivating our model, we specify the transition probabilities of the spatially detailed process. Then we demonstrate approximately that increased variance in the count of hosts per neighborhood increases the chance that a pathogen becomes spatially isolated from its vector. Next we analyze a local dispersal, mean-field model of the time

course of a vector-borne epidemic. We also develop a pair-approximation model, which incorporates greater spatial detail (Sato *et al.*, 1994; Ives *et al.*, 1998; Hiebeler, 2000), for the vector's advance. The models offer comparisons to the detailed model at different levels of host spatial heterogeneity. Then we outline our simulation experiment and report its results. Finally, we discuss generalities suggested by our analyses.

2. GENERAL ASSUMPTIONS

We designed this study for diseases that advance in the way aphids spread nonpersistent viruses over temperate crop plants (e.g., Carter and Harrington, 1991). Nonpersistent viruses are carried on or inside an aphid's mouthparts and do not replicate within aphids (cf. McElhany *et al.*, 1995). An aphid vector must successfully probe a susceptible host plant to make infection possible. That is, pathogen transmission in the absence of the vector apparently does not occur. Most movements of nonpersistent virus occur over short distances within a plant population, indicating that the pathogen is spread by apterous aphids. Aphid movements between host plants are influenced by wind speed and direction (Carter and Harrington, 1991), suggesting that neighborhood size and asymmetry depend on abiotic conditions.

Based on the example, suppose that individual hosts may recover from vector infestation, but not from pathogen infection. The vector advances from infested to uninfested hosts within a local neighborhood. Suppose the first host is also infected by the pathogen, but the second is a susceptible. Once the vector infests both host individuals, the latter host may acquire the pathogen. Hence, pathogen transmission is also spatially structured. These assumptions motivate the following model.

3. SPATIALLY DETAILED MODEL OF VECTOR-BORNE DISEASE

The environment contains J ($J \gg 1$) total sites arranged as a rectangular lattice with eight nearest-neighbor connectivity. Opposite sides of the lattice are toroidally wrapped to eliminate edge effects. Each of N sites supports a single host individual. H is the global host density; $0 < H = N/J < 1$. We list symbols used in Table 1.

We model a single growth season lasting τ time intervals (days, conveniently). Hosts neither die nor reproduce over the course of a single season. At any time t , where $0 \leq t \leq \tau$, the state of site k , $s_k(t)$, belongs to a set

TABLE 1

Model Symbols (Simulation Values Where Applicable)

Spatially detailed model	
J	Lattice size (2048)
H	Global host density (1/8, 1/4)
τ	Length of season/simulation (200)
σ_k	Interaction neighborhood around site k
δ	Neighborhood size (24, 99, 224)
α	Vector attack probability (0.14/ δ , 1.4/ δ)
μ	Host recovery probability (0.001, 0.01)
β	Pathogen transmission probability (0.01)
n_k	Number of hosts on σ_k
v_k	Number of infested hosts on σ_k
i_k	Number of infested and infected hosts on σ_k
$\psi(i)$	$1 - (1 - \beta)^i$
$\rho_v(k)$	$P[\text{Uninfested host at site } k \text{ is infested in 1 day}]$
$\rho_i(k)$	$P[\text{Infested host at site } k \text{ is infected in 1 day}]$
Vector-pathogen separation model	
g_n	$\text{Pr}[n_k = n]$
j_k	Number of uninfested and infected hosts on σ_k
θ	$\text{Pr}[\text{Host on } \sigma_k \text{ infected}]$
c_k	Number of hosts on σ_k infested by time $1/\mu$
Mean-field model	
x_t	Global density of uninfested and infected hosts
y_t	Global density of infested and infected hosts
z_t	Global density of uninfested and infected hosts
Γ	$(x_{t+1} + y_{t+1})$, total number of infested hosts, as function of (x_t, y_t, z_t)
Pair approximation	
$P[ij]$	Block probability; probability that site k has elementary state i and a randomly chosen site on σ_k has elementary state j
π	Conditional probability a randomly selected site on σ_k is occupied by a host, given that a host occupies site k
ω_t	$P_t[12]/P_t[1]$; under pair approximation, conditional probability a randomly selected site on σ_k is occupied by an infested host, given an uninfested host at site k

of five elementary states. If $s_k = 0$, site k is empty. If $s_k = 1$, the site is occupied by a host that is neither infested nor infected. If $s_k = 2$, the site is occupied by a vector-infested, but not pathogen-infested host. If $s_k = 3$, the site is occupied by a host that is both infested and infected. Finally, if $s_k = 4$, the site is occupied by an infected, but not infested, host. Figure 1 shows the five elementary states and allowable state transitions. The state of the environment at time t is $S(t) = \{s_1(t), s_2(t), \dots, s_J(t)\}$.

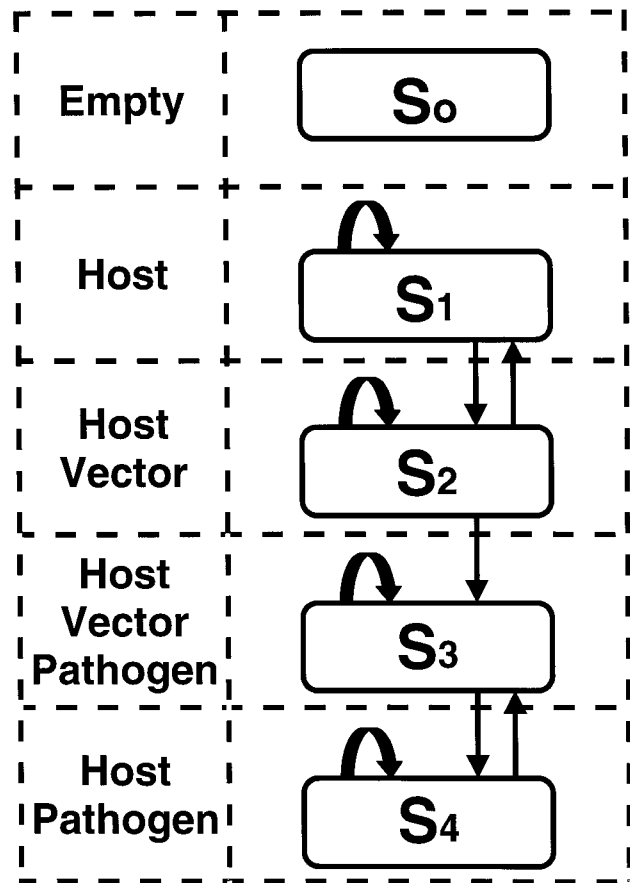


FIG. 1. Elementary states s_k and allowable transitions between states. Note that s_0 is a site hosts cannot occupy.

Transitions in $s_k(t)$ involve only the state at site k and the states of a set of nearby sites. σ_k represents the interaction neighborhood for site k . The geometry of σ_k depends on active or passive vector movements. The number of sites in σ_k (excluding k) is $\delta = |\sigma_k| - 1$. If an uninfested host occupies site k , the vector can reach that host only from infested hosts within σ_k . The disease can advance to the host at site k only if that host is infested by the vector, but still susceptible to infection *and* the host that is the source of the pathogen is not only infested, but also infested and occupies a site within σ_k . That is, the vector must infest both an infested and a nearby susceptible host for the pathogen to spread from the former to the latter.

The characterization of σ_k just described suggests the cellular-automaton form of our model's transition probabilities (Eqs. (2) and (4) below). An equivalent characterization of the neighborhood considers an infested (or infested and infected) host at site k . Then the vector can advance from site k only to uninfested hosts

on σ_k . If the host at k is infested and infected, the pathogen can spread from site k only to infested susceptibles on σ_k . If the neighborhood is symmetric (site k at the “center”), the elements of σ_k are the same under either characterization. If σ_k is asymmetric, the set of sites from which a host at k is infested differs from the set of sites to which the vector can advance from k ; the same geometry applies to the pathogen.

α is the probability, per day, that an uninfested host at site k is successfully attacked by the vector from a given infested host on σ_k . Different infested hosts within the neighborhood σ_k independently attack the uninfested host at site k ; one successful attack results in infestation. μ is the probability, per day, that an infested host recovers from the vector. Infested hosts recover independently, and recovered hosts can be reinfested.

β is the probability, per day, that an infested and infected host on σ_k transmits the pathogen to the infested host at site k . Hosts that are both infested and infected transmit the pathogen independently. Infected hosts do not recover during the growing season.

Spatial heterogeneity implies that the number of hosts per neighborhood varies. The discrete random variable n_k counts hosts occupying the δ sites within σ_k . The mean number of hosts per neighborhood is $E[n_k] = H\delta$. $V[n_k]$ is the among-neighborhood variance in the number of hosts; spatial heterogeneity increases as $V[n_k]$ increases.

3.1. Transition Rules

To develop the transition rules, we identify the presence or absence of the vector and pathogen among hosts on σ_k . Let $v(k)$ count hosts on σ_k infested by the vector, $v(k) \leq n_k$. Let $i(k)$ count the number of hosts on σ_k that are infested and also infected by the pathogen, $i(k) \leq v(k)$.

Sources of infestation act independently, so an uninfested host at site k acquires the vector in a single time interval with conditional probability

$$1 - (1 - \alpha)^v, \quad (1)$$

given that $v(k) = v$. The unconditional probability that the host at site k becomes infested in a single time interval is $\rho_v(k)$,

$$\rho_v(k) = \sum_{n=1}^{\delta} \sum_{v=1}^n [1 - (1 - \alpha)^v] \times P[v(k) = v | n_k = n] P[n_k = n]. \quad (2)$$

Pathogen infection has a similar form. Consider an infested, but uninfected host at site k . Sources of infection act independently, so the susceptible host at site k acquires the pathogen in a single time interval with conditional probability

$$\psi(i) = 1 - (1 - \beta)^i, \quad (3)$$

given that $i(k) = i$. The unconditional probability that the infested host at site k becomes infected in a single time interval is $\rho_i(k)$,

$$\rho_i(k) = \sum_{n=1}^{\delta} \sum_{v=1}^n \sum_{i=1}^v \psi(i) P[i(k) = i | v_k = v, n_k = n] \times P[v_k = v | n_k = n] P[n_k = n]. \quad (4)$$

The expressions for $\rho_v(k)$ and $\rho_i(k)$ show how variation is compounded in the transition rules. Counts of infested and infected hosts vary randomly, but each is constrained by n_k . As a consequence of spatial heterogeneity, n_k also varies randomly among neighborhoods. For any pathogen transmission probability β , the frequency of vector infestation should increase as global host density H , neighborhood size δ , or vector-infestation probability α increases, and as the recovery probability μ decreases. The incidence of disease should respond similarly.

4. SPATIAL HETEROGENEITY AND ADVANCE OF THE PATHOGEN

Heterogeneity in local host density can inhibit the spread of a vector-borne pathogen in two ways. First, host spatial heterogeneity could limit the vector's advance, constraining the pathogen indirectly. Second, heterogeneity in host abundance might increase the chance that the pathogen becomes physically separated from its vector, so that infection frequency fails to increase despite advancing vector infestation.

Our previous analyses of a directly transmitted infection, from which hosts could recover, indicate that the chance of rapid pathogen extinction increases as host spatial aggregation increases (Caraco et al., 1998). Applying the results to vector-borne disease suggests that host spatial heterogeneity should increase the probability of the vector's extinction and should decrease the frequency of infestation when the vector remains extant (see Bolker, 1999). Both effects limit the extent of pathogen infection indirectly.

Vector–pathogen separation implies that the spatial distribution of infestation and infection does not overlap, at least temporarily. Separation of the pathogen from its vector could affect an epidemic process if it occurs early in the growing season, before many hosts are infected (i.e., while chance effects remain significant). The vector might continue to infest new host individuals, while the pathogen remained isolated. If the vector fails to contact the pathogen-infected hosts or if infestation of those hosts is delayed, then the frequency of disease should be limited as a consequence.

Assuming that the pathogen and its vector might become separated, we can ask whether the probability of separation increases with host spatial heterogeneity. To do so, we assume a simple initial configuration of the interaction neighborhood. A single vector-infested host at site k is surrounded by a random number of host individuals. Some or all of these hosts may be pathogen-infected, but none are infested by the vector. Then vector–pathogen separation occurs if, by chance, host recovery at site k precedes infestation of any nearby infected host.

The host at site k is infested by the vector, but not infected by the pathogen ($s_k = 2$; see Fig. 1). n_k hosts occupy sites on σ_k ; n_k varies randomly. $P[n_k = n] = g_n$; $0 \leq n \leq \delta$, and $P[n_k > \delta] = 0$. Suppose j_k of these n_k hosts are infected by the pathogen, but not infested by its vector ($s_k = 4$). j_k is a random variable; $0 \leq j_k \leq n$, given that $n_k = n$. If $j_k < n$, the other $(n - j_k)$ hosts are neither infested nor infected ($s_k = 1$); no hosts are both infested and infected.

The j_k infected hosts represent an inoculum of the disease (e.g., hosts infected during a previous season). If $j_k = 0$, inoculation fails and vector and pathogen remain separated. If $j_k > 0$, vector–pathogen separation requires that the host at site k recover from infestation before the vector at k successfully attacks any infected host on σ_k . For simplicity, we ignore indirect infestation of infected hosts through individuals initially free of both vector and pathogen.

The number of infected hosts j_k is specified by the conditional distribution of j_k , $P[j_k = j | n_k = n]$. We analyze two conditional distributions for the number of infected hosts on σ_k . First, we assume that the elementary states of sites on σ_k are probabilistically independent; then we assume an all-or-none pathogen inoculation.

4.1. Independent Infectives

Suppose that each of the n_k hosts on σ_k is independently infected with probability θ . Then the conditional distribution of j_k is binomial with $E[j_k | n_k = n] = \theta n$.

The unconditional distribution of the number of infected hosts is a compounded binomial:

$$P[j_k = j] = \sum_{n=j}^{\delta} \frac{n!}{j!(n-j)!} \theta^j (1-\theta)^{n-j} g_n. \quad (5)$$

The unconditional expectation is $E[j_k] = \theta H \delta$.

The j_k infected hosts are susceptible to attack from the infested host at site k . For simplicity, we fix the duration of vector infestation at its expectation, $1/\mu$. Then the probability that any particular host on σ_k is not infested before the host at k recovers is $(1-\alpha)^{1/\mu}$.

Let c_k count the number of vector infestations occurring among the j_k infected hosts during $1/\mu$ time intervals. The probability of interest is $P[c_k = 0]$, the chance that the vector and pathogen remain separated. Then,

$$\begin{aligned} P[c_k = 0] &= \sum_{n=0}^{\delta} \sum_{j=0}^n [(1-\alpha)^{1/\mu}]^j P[j_k = j | n_k = n] g_n \\ &= \sum_{n=0}^{\delta} g_n \sum_{j=0}^n [(1-\alpha)^{1/\mu}]^j \frac{n!}{j!(n-j)!} \\ &\quad \times \theta^j (1-\theta)^{n-j}. \end{aligned} \quad (6)$$

Since $|(1-\alpha)^{1/\mu}| < 1$, the second sum is the probability generating function for the binomial with parameters n and θ (e.g., Feller, 1957). Substituting the binomial's generating function produces

$$P[c_k = 0] = \sum_{n=0}^{\delta} (1-\theta + \theta \xi_1)^n g_n, \quad (7)$$

where $\xi_1 = (1-\alpha)^{1/\mu}$. This last expression, Eq. (7), is the probability generating function for the distribution of n_k , which we designate as $E[\xi_2^n]$, where $\xi_2 = (1-\theta + \theta[(1-\alpha)^{1/\mu}])$. We approximate ξ_2^n with a Taylor series about $n = E[n_k]$. Taking the expectation of the first three terms yields

$$\begin{aligned} P[c_k = 0] &= E[\xi_2^{n_k}] \approx (1-\theta + \theta[(1-\alpha)^{1/\mu}])^{H\delta} \\ &\quad \times \left(1 + [\ln \xi_2]^2 \frac{V[n_k]}{2} \right), \end{aligned} \quad (8)$$

which implies that the probability of vector–pathogen separation should increase as host spatial heterogeneity increases.

4.2. Clustered Infectives

Now suppose that all or none of the hosts on σ_k are infected. Inoculation either fails or succeeds; success

implies that all n_k hosts are infected. Let $P[j_k = n | n_k = n] = \theta$, for $n = 1, 2, \dots, \delta$. The conditionally expected number of infected hosts is θn , as in the binomial. The unconditional distribution of j_k is

$$\begin{aligned} P[j_k = 0] &= g_0 + (1 - \theta)(1 - g_0) \\ P[j_k = n] &= \theta g_n; \quad n = 1, 2, \dots, \delta. \end{aligned} \quad (9)$$

As above, let c_k count infected hosts that are infested from the source at site k . $P[c_k = 0]$ is again the chance of vector–pathogen separation. Then,

$$\begin{aligned} P[c_k = 0] &= g_0 + (1 - \theta)(1 - g_0) \\ &+ \theta \sum_{n=1}^{\delta} [(1 - \alpha)^{1/\mu}]^n g_n \\ &= 1 - \theta + \theta \sum_{n=0}^{\delta} [(1 - \alpha)^{1/\mu}]^n g_n. \end{aligned} \quad (10)$$

The sum in the last expression is the probability generating function for the $P[n_k = n]$, $E[\xi_1^n]$, where $\xi_1 = (1 - \alpha)^{1/\mu}$.

Approximating $E[\xi_1^n]$ with a Taylor series about $n = E[n_k]$ and taking the expectation of the first three terms gives

$$\begin{aligned} P[c_k = 0] &= 1 - \theta + \theta E[\xi_1^{n_k}] \approx 1 - \theta + \theta(1 - \alpha)^{H\delta/\mu} \\ &\times \left(1 + [\ln \xi_1]^2 \frac{V[n_k]}{2} \right). \end{aligned} \quad (11)$$

As above, $P[c_k = 0]$ should increase with $V[n_k]$.

The approximate analysis of $P[c_k = 0]$ merely suggests that an initial vector–pathogen separation may be more likely as host spatial heterogeneity increases. If spatial heterogeneity in host density constrains the vector's global advance (Duryea *et al.*, 1999), then the expected duration of an isolated pathogen-infected host from the vector should not decrease as host spatial heterogeneity increases. Hence, the chance that vector–pathogen separation limits pathogen prevalence should increase with host spatial variance.

5. MEAN FIELD ANALYSIS

Spatially explicit models make a number of novel ecological predictions (Levin *et al.*, 1997), some of which contradict results of traditional, aspatial models (Kareiva, 1990; Holmes, 1997; Law and Dieckmann, 2000). The complexity of spatially detailed dynamics is

due in part to spatial correlations between states of nearby sites (Wilbur *et al.*, 1986; Matsuda *et al.*, 1992; Sato *et al.*, 1994; Ellner *et al.*, 1998). To see effects of this dependence, we approximate the detailed model by neglecting spatial correlation; the resulting mean-field analysis serves as a comparison to the detailed model (Harada *et al.*, 1995; Bolker and Pacala, 1997; Hiebeler, 1997, 2000).

We adopt what Hiebeler (1997, 2000) terms the local-dispersal mean-field approximation. We retain the assumption that infestation and infection have a localized, neighborhood structure. But we assume no spatial correlations between elementary states of different lattice sites. Independence of different hosts' states lets us treat host densities as probabilities of finding a given host in each elementary state.

x_t ($0 < x_t < H$) represents the global density of hosts infested by the vector, but not infected by the pathogen ($s_k = 2$), at time t . y_t represents the global density of hosts that are both infested and infected at time t ($s_k = 3$). z_t is the global density of hosts that are infected by the pathogen, but not infested by the vector ($s_k = 4$), at time t ; these hosts were formerly infested by the vector and have recovered. So, for any t , $0 \leq t \leq \tau$, the global density of hosts neither infested nor infected is $(H - x_t - y_t - z_t)$.

Infestation and infection processes involving the host at site k are restricted to the neighborhood σ_k . The assumption that the states of different sites are probabilistically independent implies that the state counts across the δ sites about k have a multinomial distribution. Therefore, the marginal count for each elementary state has a binomial distribution, which we use in the mean-field model.

The mean-field density of infested, but uninfected, hosts has the following equation:

$$\begin{aligned} x_{t+1} &= F_x(x_t, y_t, z_t) \\ &= x_t(1 - \mu) \sum_{n=0}^{\delta} \frac{\delta!}{n!(\delta - n)!} y_t^n (1 - y_t)^{\delta - n} \\ &\quad \times (1 - \beta)^n + (H - x_t - y_t - z_t) \sum_{n=0}^{\delta} \frac{\delta!}{n!(\delta - n)!} \\ &\quad \times (x_t + y_t)^n [1 - (x_t + y_t)]^{\delta - n} [1 - (1 - \alpha)^n] \\ &= x_t(1 - \mu)(1 - \beta y_t)^\delta + (H - x_t - y_t - z_t) \\ &\quad \times [1 - (1 - \alpha[x_t + y_t])^\delta]. \end{aligned} \quad (12)$$

The first term accounts for infested hosts that do not recover and are not infected. The second term represents infestation of hosts that are neither infested nor infected.

Using summed binomial probabilities as in F_x , the mean-field density of infested and infected hosts has the equation

$$\begin{aligned} y_{t+1} &= F_y(x_t, y_t, z_t) \\ &= x_t(1-\mu)[1-(1-\beta y_t)^\delta] + y_t(1-\mu) \\ &\quad + z_t[1-(1-\alpha[x_t + y_t])^\delta]. \end{aligned} \quad (13)$$

The respective terms represent infection of infested hosts, hosts that are both infested and infected and do not recover, and infestation of previously infected hosts.

For the mean-field density of infected, but not infested, hosts, we have

$$z_{t+1} = F_z(x_t, y_t, z_t) = \mu y_t + z_t(1-\alpha[x_t + y_t])^\delta. \quad (14)$$

The first term represents recovery from infestation. The second counts pathogen-infected hosts that do not become reinfested.

For the total mean-field density of infested hosts, we have

$$\begin{aligned} (x_{t+1} + y_{t+1}) &= F(x_t, y_t, z_t) \\ &= (x_t + y_t)(1-\mu) + (H - x_t - y_t) \\ &\quad \times [1-(1-\alpha[x_t + y_t])^\delta]. \end{aligned} \quad (15)$$

The equation for the total mean-field density of pathogen-infected hosts is simple, since hosts do not recover from infection:

$$(y_{t+1} + z_{t+1}) = x_t(1-\mu)[1-(1-\beta y_t)^\delta] + y_t + z_t. \quad (16)$$

We computed x_t , y_t , and z_t over the course of the finite growing season (τ days) for each (H, α, δ, μ) -combination used to simulate the spatially detailed model. Below we compare simulations to the corresponding mean-field dynamics. In general, the mean-field results showed that y_{200} (infested and infected hosts) exceeded 0.9 when the vector-attack probability α was at its higher level. For lower α , y_{200} tended to increase, and z_{200} tended to decrease, as neighborhood size δ increased, and as infestation-recovery probability μ decreased. In the Appendix we analyze the mean-field equilibria and their local stability.

6. PAIR APPROXIMATION

The local-dispersal mean-field model assumes that ecological interactions have a neighborhood structure,

but it does not allow correlations between states of nearby sites. A model incorporating limited spatial correlation should better approximate the spatially detailed dynamics (e.g., Ellner *et al.*, 1998), so we consider a pair approximation (Ives *et al.*, 1998; Hiebeler, 2000) for the vector's dynamics.

A pair approximation analyzes probabilities for the state combinations of paired, neighboring sites. The dynamics of the frequencies of the various "block pairs" quantify a degree of local spatial correlation that mean-field models ignore (Sato *et al.*, 1984; Harada *et al.*, 1995; Hiebeler, 1997; Ives *et al.*, 1998). By simply summing block-pair probabilities, frequencies of the elementary states are obtained.

$P[ij]$ represents a block probability; $P[ij]$ is the probability that the state at site k is i , and the state at another, randomly chosen site on σ_k is j . The spatially detailed model of vector-borne infection assumes five elementary states; hence there are 25 block probabilities. By spatial symmetry we can assume $P[ij] = P[ji]$, reducing the problem to 15 block probabilities. Equality constraints permit a further reduction to 12 block probabilities, but the dimensionality remains too large to be of interest. However, the pair approximation to the host-vector dynamics is manageable and offers some biological insight.

The host-vector interaction involves three of the elementary states; a site may be empty (s_0), occupied by an uninfested host (s_1), or occupied by an infested host (s_2). There are then 9 block probabilities, which reduce to 6 by spatial symmetry: $P[00]$, $P[01]$ ($= P[10]$), $P[02]$ ($= P[20]$), $P[11]$, $P[12]$ ($= P[21]$), and $P[22]$. The block probabilities must sum to 1:

$$\sum_{i=0}^2 P[ii] + 2 \sum_{i=0}^1 \sum_{j>i} P[ij] = 1. \quad (17)$$

Since global host density H is fixed, the proportion of sites that are empty, $P[0]$, must be

$$P[0] = \sum_{j=0}^2 P[0j] = 1 - H. \quad (18)$$

To introduce host spatial dispersion to the pair approximation, let π be the conditional probability that a host occupies a randomly selected site on σ_k , given that a host occupies site k . π depends on host dispersion and can depend on neighborhood size, but not on the vector's presence or absence. In general, host aggregation increases the

average number of neighbors per host, so π should not decrease as host spatial heterogeneity increases.

By spatial symmetry, $P[01] + P[02] = P[10] + P[20]$. The latter sum is the probability that site k is occupied and a randomly selected site on σ_k is empty. Then,

$$P[10] + P[20] = H(1 - \pi). \quad (19)$$

Using (18) and spatial symmetry, we have

$$P[0] + P[00] + H(1 - \pi) = 1 - H.$$

So,

$$P[00] = 1 - H(2 - \pi), \quad (20)$$

which requires $2 - \pi < H^{-1}$ and fixes the block probability for neighboring empty sites, $P[00]$.

Expressions (17), (19), and (20) together allow specification of the pair-approximation model by writing equations for the dynamics of three block probabilities. As above, μ is the probability that an infested host recovers from the vector in a single time interval; recovery at site k is independent of the states at nearby sites. We apply the assumptions of pair approximation to the infestation process. Pair approximation assumes that the correlation between two neighboring sites is independent of any randomly selected third site (Nakamura *et al.*, 1997; Ives *et al.*, 1998; Hiebeler, 2000). Suppose that neighboring sites k and q form a [11] block pair. Then $s_k = s_q = 1$; sites k and q are each occupied by an uninfested host. The host at site k may become infested if one or more of the $(\delta - 1)$ sites on σ_k is occupied by an infested host. In general, spatial correlation implies that the state probabilities of a randomly selected site $r \in \sigma_k$ depend conditionally on the states of sites k and q , both of which are known. Pair approximation, in our example, assumes that the correlation between sites k and r is independent of the state at site q . That is, pair approximation assumes

$$P[s_r | s_k, s_q] = P[s_r | s_k].$$

So, recall that α is the probability that the vector advances from an infested host on σ_k to infest a host at site k . Let ω_t represent the time-dependent conditional probability that a randomly selected site on σ_k is occupied by an infested host, given that an uninfested host occupies site k . Then, $P_t[12] = P_t[1] \omega_t$, where $P_t[1]$ is the global frequency of uninfested hosts at time t . So,

$\omega_t = P_t[12]/P_t[1]$. Under pair approximation, the probability that an uninfested host at site k is not infested by vector advance from any of the neighboring sites on σ_k , whose states are unknown, is $(1 - \alpha\omega_t)^\delta$.

6.1. Pair-Approximation Dynamics

We track the pair approximation through the dynamics of $P_t[01]$, $P_t[12]$, and $P_t[22]$. First, consider the block pair [01]. Using Hiebeler's (2000) representation of transition probabilities,

$$P_{t+1}[01] = P_t[01] P[01 \rightarrow 01] + P_t[02] P[02 \rightarrow 01].$$

A [01] block pair may remain unchanged, and the infested host of a [02] block may recover. Then,

$$P_{t+1}[01] = P_t[01](1 - \alpha\omega_t)^{\delta-1} + P_t[02] \mu. \quad (21)$$

The exponent is $(\delta - 1)$ since we know that one of the neighbors of the uninfested host (the other member of the block pair) cannot be a source of vector infestation.

Second, consider the block pair [12]:

$$\begin{aligned} P_{t+1}[12] &= P_t[11] P[11 \rightarrow 12] + P_t[22] P[22 \rightarrow 12] \\ &\quad + P_t[12] P[12 \rightarrow 12] \\ &\quad + P_t[21] P[21 \rightarrow 12]. \end{aligned}$$

A [12] block may arise from a [11] block if a host at site k remains uninfested while the vector infests the host at the other site of the block pair. A [22] block becomes a [12] block if the infested host at site k recovers while the vector persists at the other site. A [12] block remains unchanged if the host at site k avoids infestation and the vector persists at the other site. Finally, a [21] block becomes a [12] block if the host at site k loses the vector and the vector infests the host at the other site of the block pair. The resulting difference equation is

$$\begin{aligned} P_{t+1}[12] &= P_t[11](1 - \alpha\omega_t)^{\delta-1} [1 - (1 - \alpha\omega_t)^{\delta-1}] \\ &\quad + P_t[22] \mu(1 - \mu) \\ &\quad + P_t[12](1 - \alpha)(1 - \alpha\omega_t)^{\delta-1} (1 - \mu) \\ &\quad + P_t[21] \mu[1 - (1 - \alpha)(1 - \alpha\omega_t)^{\delta-1}]. \quad (22) \end{aligned}$$

Recall that $P_t[12] = P_t[21]$. The transitions let vector infestation precede recovery, as in the spatially detailed model. Given a [12] block, note that the probability that the susceptible host at site k is not infested is $(1 - \alpha)(1 - \alpha\omega_t)^{\delta-1}$. We know that the vector is present at the second site of the block pair, but the states of the

remaining $(\delta - 1)$ neighboring sites are unknown. Hence, the latter infestation probabilities depend on δ . A similar consideration applies to the block transition [21 \rightarrow 12].

For the block pair [22] we have

$$P_{t+1}[22] = P_t[11] P[11 \rightarrow 22] + 2P_t[12] P[12 \rightarrow 22] + P_t[22] P[22 \rightarrow 22].$$

The second term is doubled since $P_t[12] = P_t[21]$, and $P[12 \rightarrow 22] = P[21 \rightarrow 22]$. The resulting difference equation is

$$\begin{aligned} P_{t+1}[22] &= P_t[11][1 - (1 - \alpha\omega_t)^{\delta-1}]^2 \\ &+ P_t[22](1 - \mu)^2 \\ &+ 2P_t[12] \\ &\times [1 - (1 - \alpha)(1 - \alpha\omega_t)^{\delta-1}](1 - \mu). \quad (23) \end{aligned}$$

In the transition [11 \rightarrow 22] the hosts are infested independently, hence the squared term.

We computed the pair-approximation equations for each (H, α, δ, μ) combination used to simulate the spatially detailed model. We obtained π , the conditional probability that a host occupies a randomly selected site on σ_k , given that a host occupies site k , from the simulation's host dispersions (see below). Since π depended on host dispersion, we calculated the pair-approximation dynamics for different randomly generated host dispersions separately. For many parameter combinations the vector advanced more slowly under pair approximation than under the mean-field assumption. For a given spatial dispersion of hosts, pair approximation captures some of the effect of spatial clustering of the vector, and clustering can locally reduce the density of hosts susceptible to vector infestation (Caraco *et al.*, 1998; Ives *et al.*, 1998).

7. SIMULATIONS

Our simulations used software designed for studying spatially explicit population dynamics (Maniatty *et al.*, 1994,1998). Simulations were conducted on a MasPar MP-1 parallel computer. Lattice size was constant, $J = 2048$ sites. The lattice was wrapped to eliminate edge effects. The duration of each simulation was fixed at $\tau = 200$ iterations, to model a growth season. During each iteration of the model, the sequence of probabilistic transitions was infestation by the vector, infection by the pathogen, and recovery by infested hosts. Hosts infested at time t remained so for at least one time interval. We

recorded the state of every host at each time t during simulations.

We simulated two global host densities, $H = 1/8$ and $1/4$, termed low and high density. For each global density, we simulated three neighborhood sizes, $\delta = 24, 99$, and 224 . Interaction neighborhoods were asymmetric, to model a parasitic vector driven by convection or responding to a gradient. Suppose the vector had infested a host occupying the site with coordinates (x, y) . Then the asymmetry implies that the vector could advance from that site to infest only those uninfested hosts that reside on the square with opposite corner $(x - [\delta + 1]^{1/2}, y - [\delta + 1]^{1/2})$. We simulated four different host spatial dispersions.

Agricultural. Hosts were arrayed in parallel rows; the distance between rows was constant for given global density. This is the most spatially homogeneous dispersion.

Statistically uniform. We partitioned the lattice into $J/4$ cells. For low host density, hosts were randomly assigned to half of the cells; other cells were left empty. For high density each cell was assigned a single host. The location of a host within a cell was assigned randomly. As a convenience, we call this dispersion "uniform," but note that the spatial array of host individuals is more heterogeneous than the agricultural dispersion.

Random and independent. We simulated a Poisson forest (e.g., Diggle, 1983). As a convenience, we refer to this dispersion as "random."

Clumped. The N hosts were assigned to aggregations at contiguous sites; different aggregations did not make contact. The relative frequencies of aggregation size followed a 0-truncated negative binomial probability function (Cohen, 1971). The clumped dispersion is the most spatially heterogeneous. Figure 2 shows the four host arrays for the lower global density.

To verify that the dispersions produced different levels of host spatial heterogeneity, we compared contact distributions (Mollison, 1977). We randomly selected 100 focal hosts without replacement from each array. For the programmed global densities and dispersions, we counted the number of hosts the vector could reach from each focal host. The variance to mean ratios of the number of hosts per neighborhood increased significantly across programmed dispersions, and the variance to mean ratio of the random dispersion is very close to the theoretical value of 1.0. Figure 3a shows the variance to mean ratios, for each combination of host dispersion and neighborhood size, for low global density. Figure 3b does the same for the larger global host density.

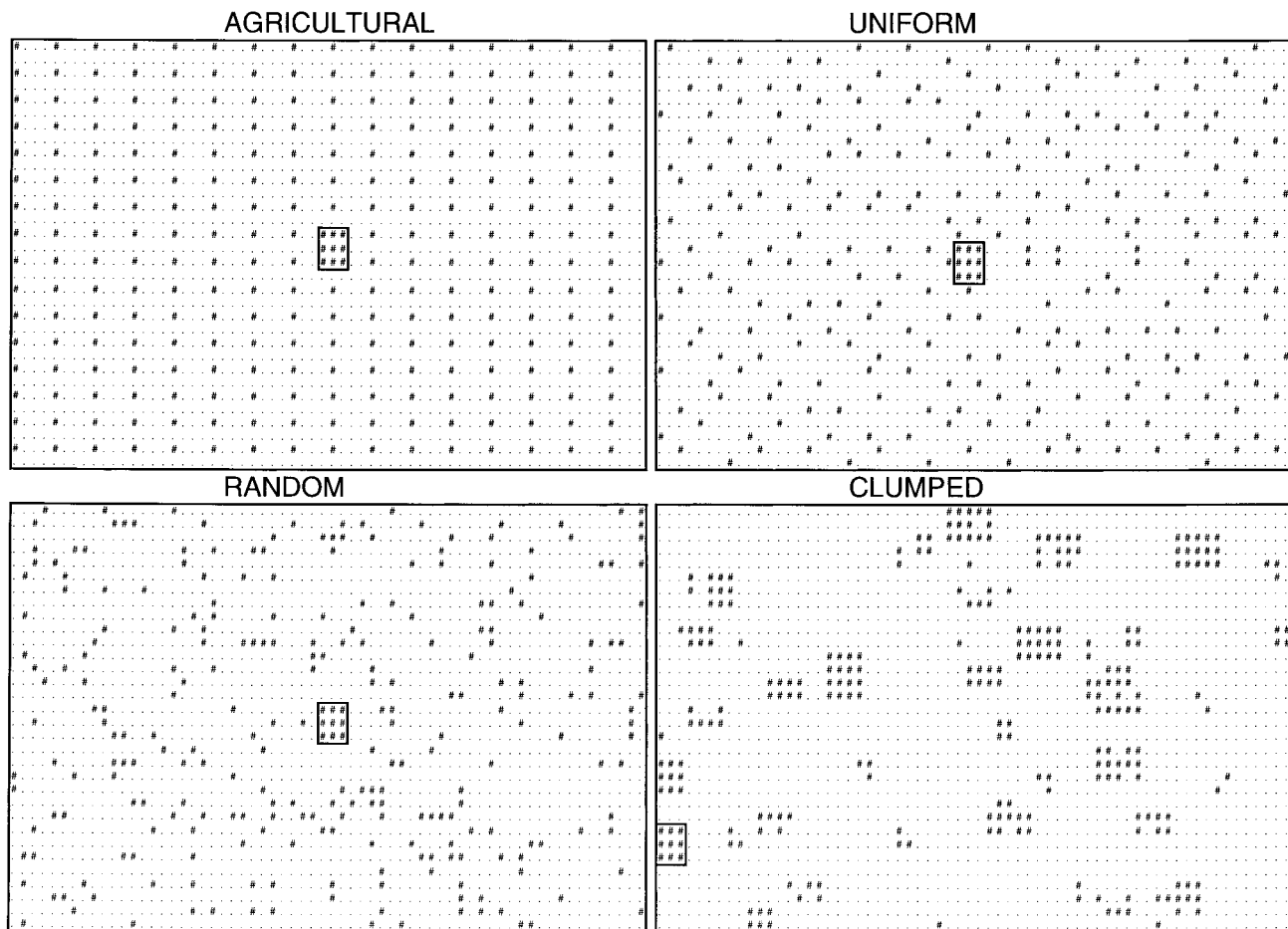


FIG. 2. Host dispersions used in simulations, low global host density. Initially, nine hosts within a block are infested and infected; all other hosts are neither infested nor infected.

Simulations began with an inoculum of nine infested and infected hosts placed on the lattice as a 3×3 square. These hosts defined the initial condition for computing the mean-field dynamics and the pair approximation, but were excluded from other analyses of vector and pathogen prevalence. In most simulations, the inoculum was placed randomly. For simulations involving the smallest neighborhood size, low host density, and clumped host dispersion (only 4 % of the total), we placed the inoculum randomly in one of several locations close to uninfested/uninfected hosts. In all of our simulations, the inoculum's position insured that the vector and pathogen could spread beyond their initial locations.

For each neighborhood size, the two levels of α were adjusted so that the product $\alpha\delta$ took values very close to 0.14 and 1.4 for each δ . This controls the vector's basic reproductive rate (e.g., Holmes, 1997), $(\alpha/\mu) E[n_k] = \alpha H\delta/\mu$, across neighborhood size. Each parameter

combination was repeated with two random number sequences; the total number of simulations was 192.

7.1. Vector Infestation

To characterize effects of host dispersion on infestation, we defined any two infested hosts occupying immediately neighboring sites at $t = 200$ as belonging to the same vector patch. Figure 4 plots mean vector-patch size and mean number of vector patches for low global host density. Each entry is an average for one of the three neighborhood sizes. Of course, the different host dispersions have different maxima for both mean vector-patch size and patch number. But if all hosts are infested, each combination satisfies (patch size) \times (patch number) = total hosts (N).

At low host density and low $\alpha\delta$ (Fig. 4a), vector patches on agricultural hosts are necessarily small, but

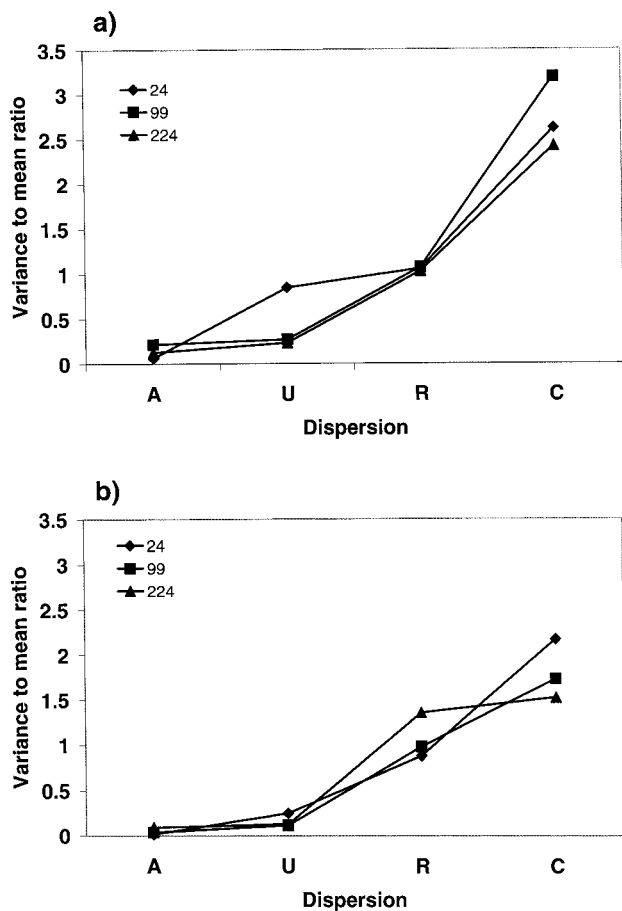


FIG. 3. Variance to mean ratios of contact distributions. Host spatial heterogeneity is minimal in the agricultural array and maximal for the clumped array. Neighborhood sizes are $\delta=24$ (diamond), 99 (square), and 224 (triangle). (a) Low global host density. (b) High global host density.

relatively numerous. When the hosts are clumped; the vector forms the largest patches on average, but their numbers are so small that the average frequency of infestation declines. A qualitatively similar pattern emerges at low global density and high $\alpha\delta$ (Fig. 4b). Clumped hosts again produce the largest vector patches, but the patches are so few that the mean infestation frequency remains the smallest. Host clumping aggregates the vector, so that vector “attacks” are more often directed at already infested hosts (Ives *et al.*, 1998). Host clumping also leaves gaps in the spatial array of hosts, which slow down the global advance of the vector (Caraco *et al.*, 1998; Neuhauser, 1998).

At high host density and low $\alpha\delta$, vector patches on agricultural hosts coalesce, so that mean patch size is now largest for the agricultural dispersion. But clumped

hosts still produce the lowest level of infestation. When both global density and $\alpha\delta$ are at the higher level, significant effects of host dispersion disappear.

7.2. Pathogen Infection

Above, we suggested three views of the epidemic process. The vector might fail to advance, limiting pathogen infection. If the vector should infest a significant fraction of the host population, the pathogen may advance with the vector. Or, vector–pathogen separation may limit pathogen infection despite the vector’s advance. In the first two cases, the frequency of infection should be relatively close to the frequency of infestation; in the last case (separation) infestation frequency should exceed infection frequency.

Figures 5a–5d plot the difference between infestation and infection frequencies at the end of simulation against the infestation frequency. Each plot shows all simulations for a given host dispersion, for one random number sequence. Results for the other set of random numbers are quite similar. In the majority of simulations the difference between infestation and infection frequency is close to 0, so that the extent of infection follows from the level of vector infestation. However, in about 1/8 of the simulations infestation frequency exceeds 0.8, while infection frequency remains much smaller (hence a large difference is plotted). For the latter results the elementary-state counts reveal vector–pathogen separation. As indicated in Fig. 5, separation can occur under any of the four host dispersions and hence need not be more likely as host aggregation increases. However, the degree of vector–pathogen separation, when it occurs, is greatest for clumped hosts.

Overall, 20 of 21 simulations (both random number sets) where vector and pathogen separated were associated with the greater vector-attack probability (α) and the smallest neighborhood size (δ). The greater α allows the vector to advance to a high frequency of infestation. The smaller neighborhood isolates an initial pocket of pathogen infection from a greater number of vector-infested hosts, increasing the likelihood of chance separation.

Table 2 shows mean frequencies of pathogen infection at $t=200$ for each host spatial dispersion. Separate entries are given for combinations of global host density ($H=1/8, 1/4$) and vector recovery probability ($\mu=0.001, 0.01$). Observed infection frequencies are greatest for agriculturally arrayed hosts and least for clumped hosts. That is, the frequency of vector-borne infection declines as host spatial heterogeneity increases. Although

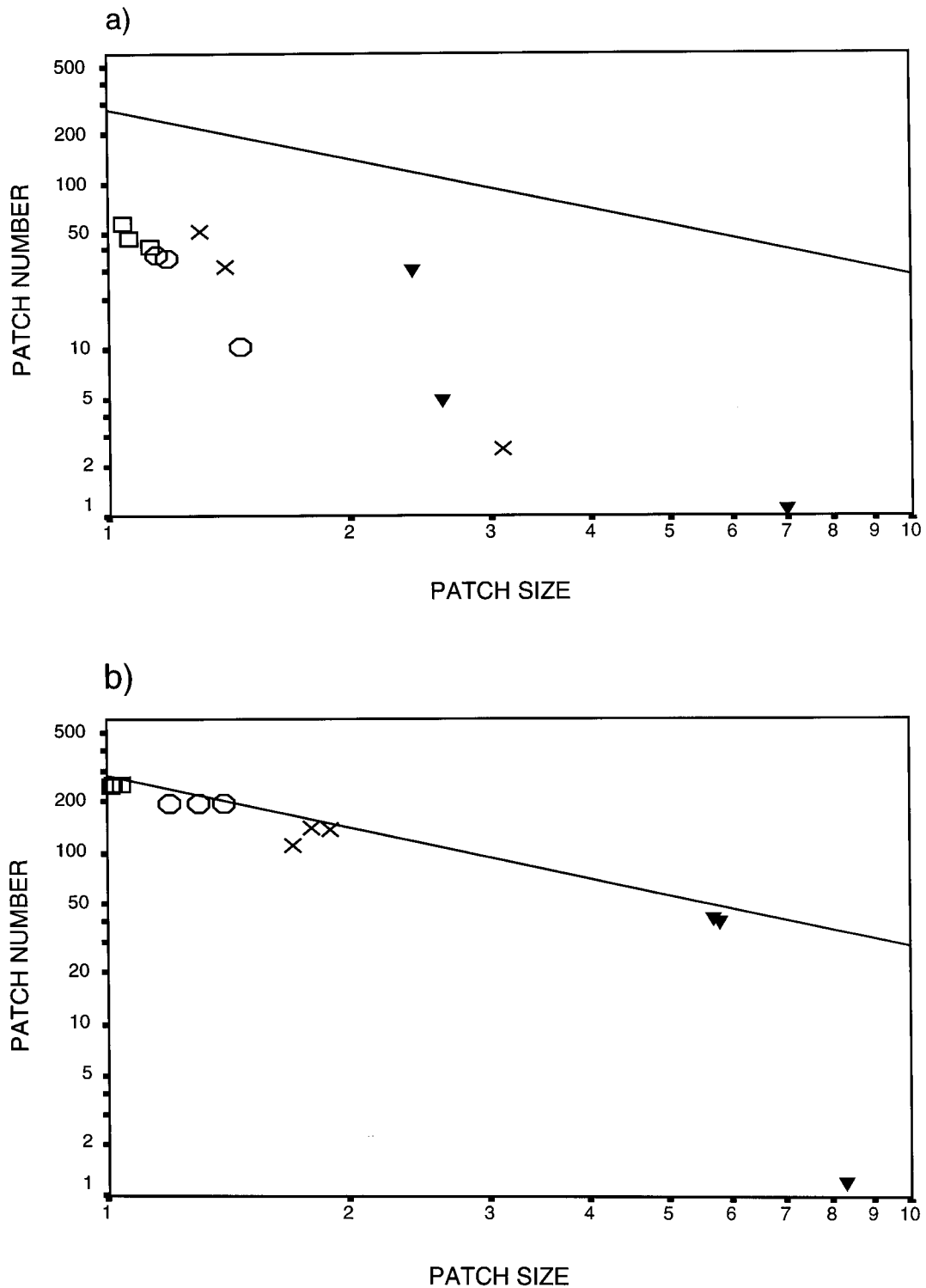


FIG. 4. Mean size and mean number of vector patches, low global host density. Axes are scaled logarithmically. The continuous line shows combinations where each host is infested. Each entry is the mean for one of three neighborhood sizes; averages are taken at the end of simulations ($t = 200$). Host spatial dispersions are agricultural (square), statistically uniform (circle), random (x), and clumped (triangle). (a) Low $\alpha\delta$. (b) High $\alpha\delta$.

TABLE 2

Average Frequencies of Pathogen Infection at $t = 200$

	Host spatial dispersion			
	A	U	R	C
$H = 1/8, \mu = 10^{-3}$	0.56	0.44	0.43	0.4
$H = 1/8, \mu = 10^{-2}$	0.44	0.38	0.37	0.31
$H = 1/4, \mu = 10^{-3}$	0.85	0.68	0.68	0.59
$H = 1/4, \mu = 10^{-2}$	0.72	0.57	0.59	0.46

Note. Entries are averaged over neighborhood size (δ), vector-attack probability (α), and replications. H is global host density, μ is probability of recovery from vector infestation; dispersions are agricultural (A), statistically uniform (U), random and independent (R), and clumped (C).

not shown in Table 2, reduction in the extent of infection as host aggregation increases is relatively strong for the two smaller neighborhood sizes and weaker at the largest δ , where the dynamics approach homogeneous mixing.

We conducted an ANOVA on infection frequencies at $t = 200$ for both global densities, after transforming frequencies by the arcsine square root method. We combined results across random number sequences and levels of the recovery probability μ . Treatments were host spatial dispersion (four levels), vector attack probability (two levels), and neighborhood size (three levels). Table 3 reports the ANOVA results for low host density. Neighborhood size interacts strongly with host dispersion (and vector-attack probability). That is, the level of vector-borne infection is especially low when the interaction neighborhood is small and hosts are clumped. Scheffé's multiple comparison (e.g., Hays, 1994) revealed that infection among agriculturally arrayed hosts is significantly greater ($P < 0.05$) than among any other dispersion. Statistically uniform and random host dispersions do not differ significantly in infection frequency. Infection among clumped hosts is significantly less ($P < 0.05$) than among any other host spatial dispersion.

For high host density, the ANOVA results were similar to those for low density (Table 3). Neighborhood size again interacts with host spatial dispersion; small neighborhood size and clumped hosts combine to limit the level of infection. Scheffé's multiple comparison again found infection among agriculturally arrayed hosts to be significantly greater ($P < 0.05$) than among any other host dispersion. Statistically uniform and random dispersions did not differ significantly. Infection among clumped hosts was significantly less ($P < 0.05$) than among any other spatial dispersion.

TABLE 3

ANOVA Results, Infection Frequencies

Effect	d.f. effect	F	Significance
Low host density			
Dispersion	3	$F_{3,72} = 23.7$	$P < 10^{-4}$
α	1	$F_{1,72} = 1276$	$P < 10^{-4}$
δ	2	$F_{2,72} = 420.2$	$P < 10^{-4}$
Disp. \times α	3	$F_{3,72} = 4.9$	$P < 10^{-2}$
Disp. \times δ	6	$F_{6,72} = 14.4$	$P < 10^{-4}$
$\alpha \times \delta$	2	$F_{2,72} = 161.8$	$P < 10^{-4}$
Disp. \times $\alpha \times \delta$	6	$F_{6,72} = 1.7$	NS
Error mean square = 0.013			
High host density			
Dispersion	3	$F_{3,72} = 32.8$	$P < 10^{-4}$
α	1	$F_{1,72} = 654$	$P < 10^{-4}$
δ	2	$F_{2,72} = 265$	$P < 10^{-4}$
Disp. \times α	3	$F_{3,72} = 0.927$	NS
Disp. \times δ	6	$F_{6,72} = 16.3$	$P < 10^{-4}$
$\alpha \times \delta$	2	$F_{2,72} = 7.8$	$P < 10^{-2}$
Disp. \times $\alpha \times \delta$	6	$F_{6,72} = 6.9$	$P < 10^{-4}$
Error mean square = 0.015			

The plots in Figs. 6a and 6b show the cumulative percentage of simulations where the infection frequency at $t = 200$ was less than or equal to the abscissa value. Each plot indicates that limited epidemics, i.e., low frequencies of pathogen infection, are more common when hosts have a clumped dispersion.

7.3. Mean-Field Dynamics, Pair Approximation, and Simulation

We computed the state variables of the mean-field model over 200 iterations for each parameter combination used in simulation. Initial conditions for the mean-field dynamics equaled the global initial densities used in each simulation: $x_0 = 0$, $y_0 = 0.0044$, and $z_t = 0$. The pair approximations required more extensive computation because initial conditions depended on the level of host spatial heterogeneity. We calculated π , $P_0[10]$, $P_0[12]$, and $P_0[22]$ for the uniform, random, and clumped host arrays separately, at both low and high global density. Since pair approximation is defined in terms of spatial probabilities, we excluded the deterministic agricultural array from this analysis. We computed the block probabilities over 200 iterations for each parameter combination used in simulation.

By first considering vector infestation without regard to the level of infection, we can compare simulations to

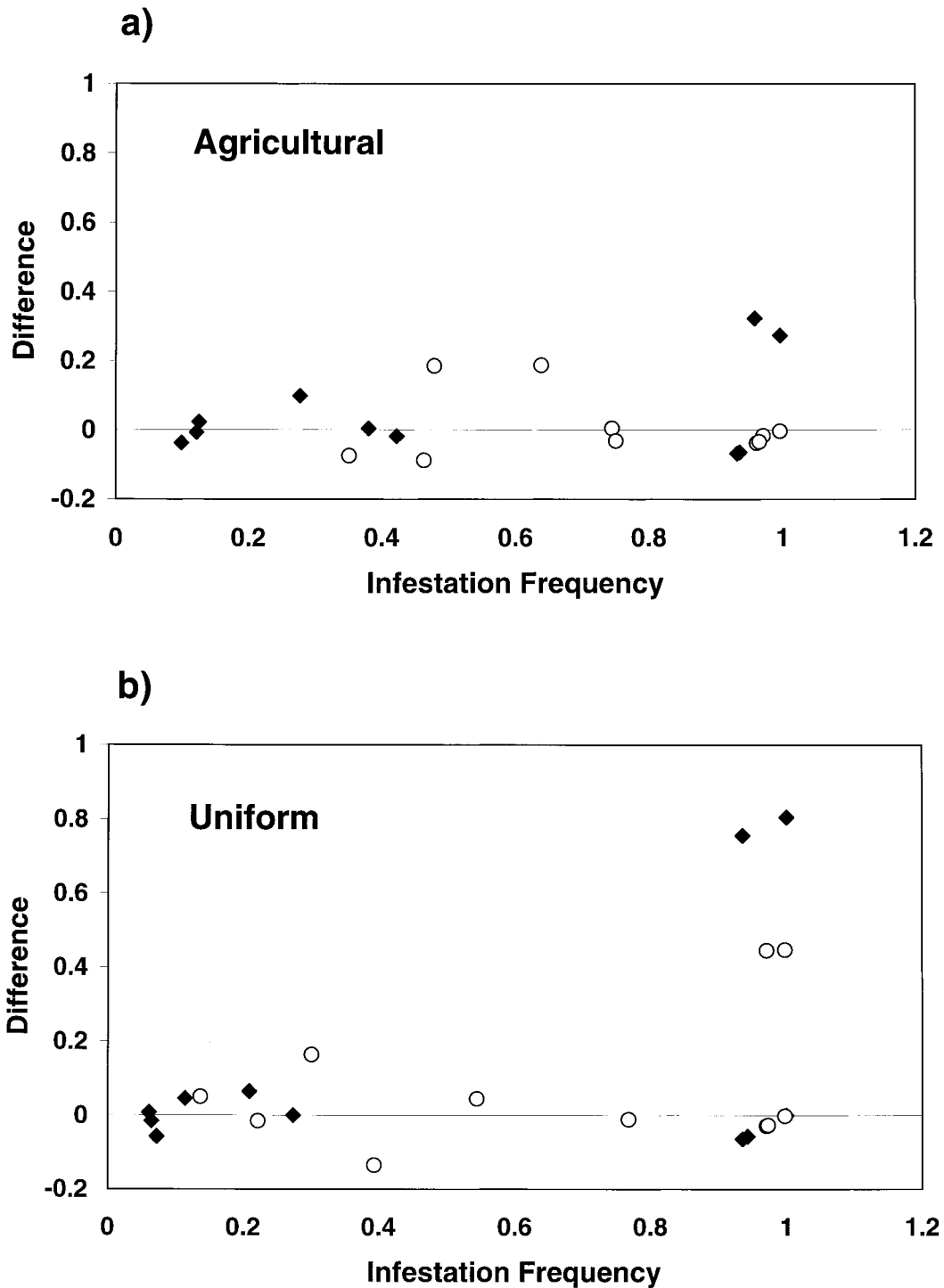


FIG. 5. Vector infestation and pathogen infection. Abscissa is the frequency of vector infestation at the end of simulations ($t = 200$). The ordinate is the difference, vector infestation frequency minus pathogen infection frequency, at the end of simulations ($t = 200$). Closed diamonds are low global host density; open circles are high global host density. If both infestation frequency and the difference are large, the vector has advanced, but the disease prevalence has remained relatively small. In these cases, vector-pathogen separation has occurred; only a small fraction of infested hosts is also infected. (a) Agricultural array. (b) Uniform host dispersion. (c) Random array. (d) Clumped array.

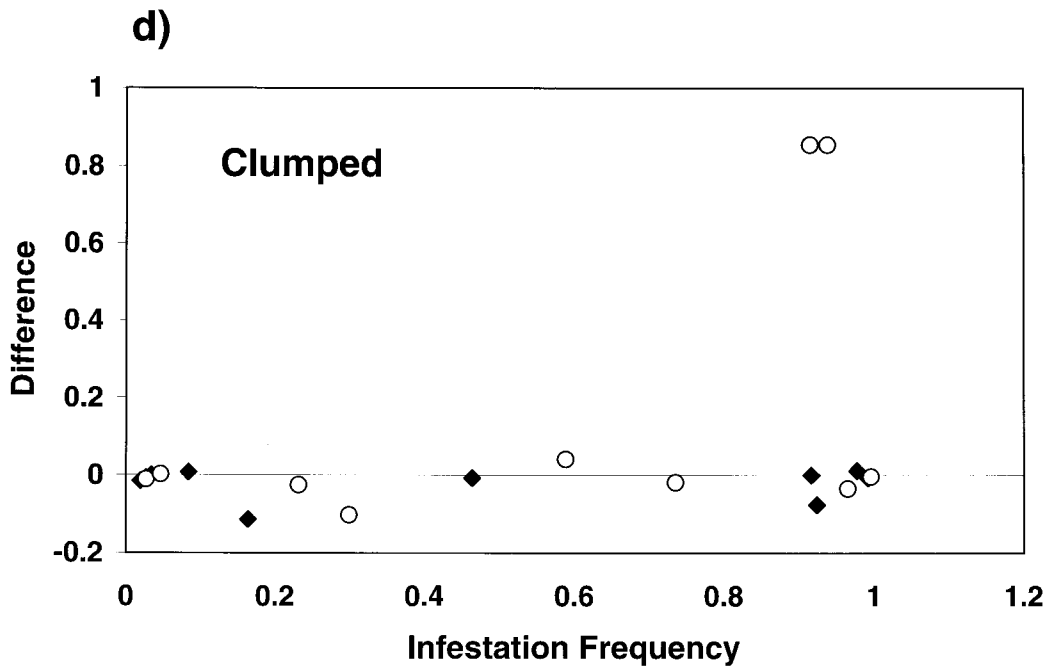
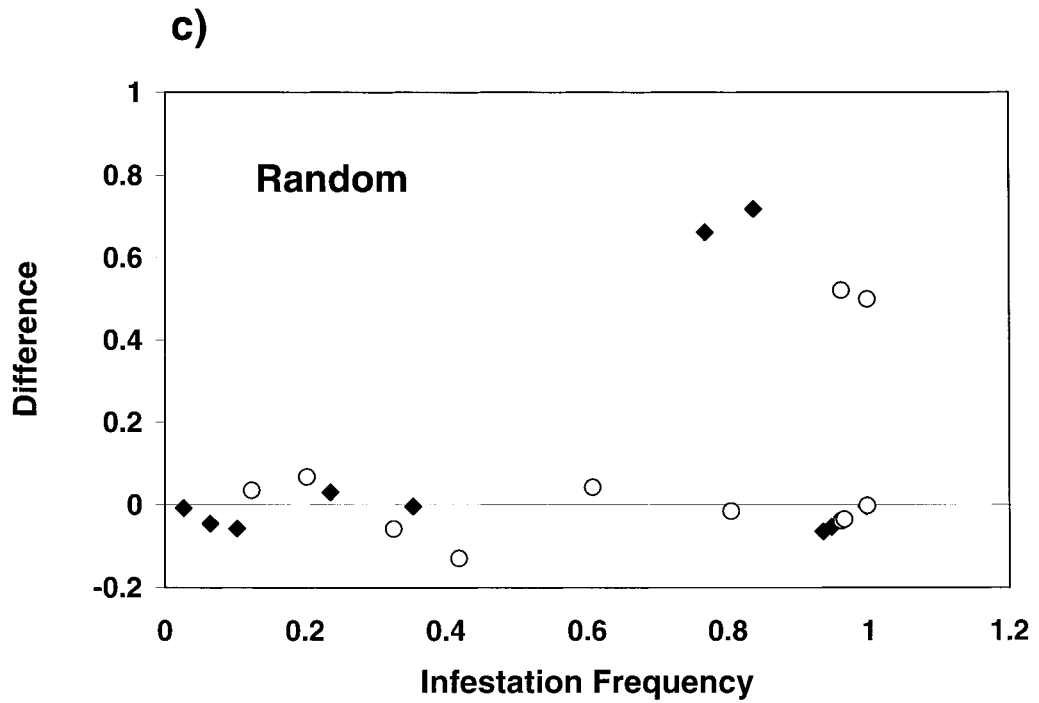


FIG. 5—Continued

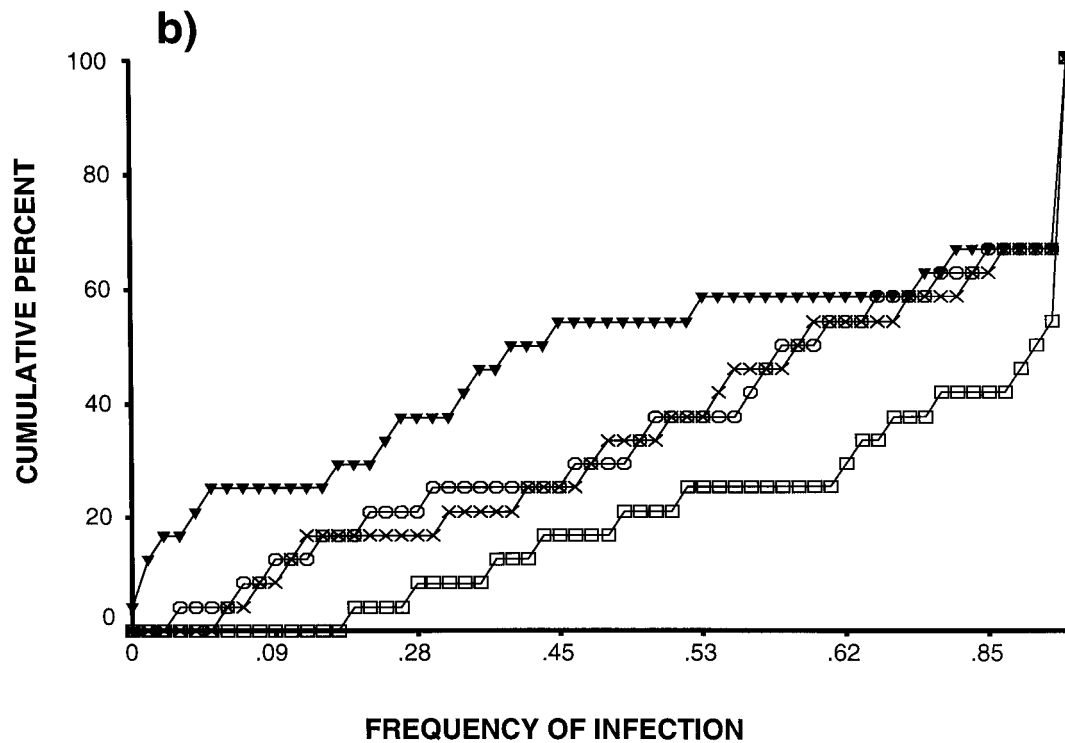
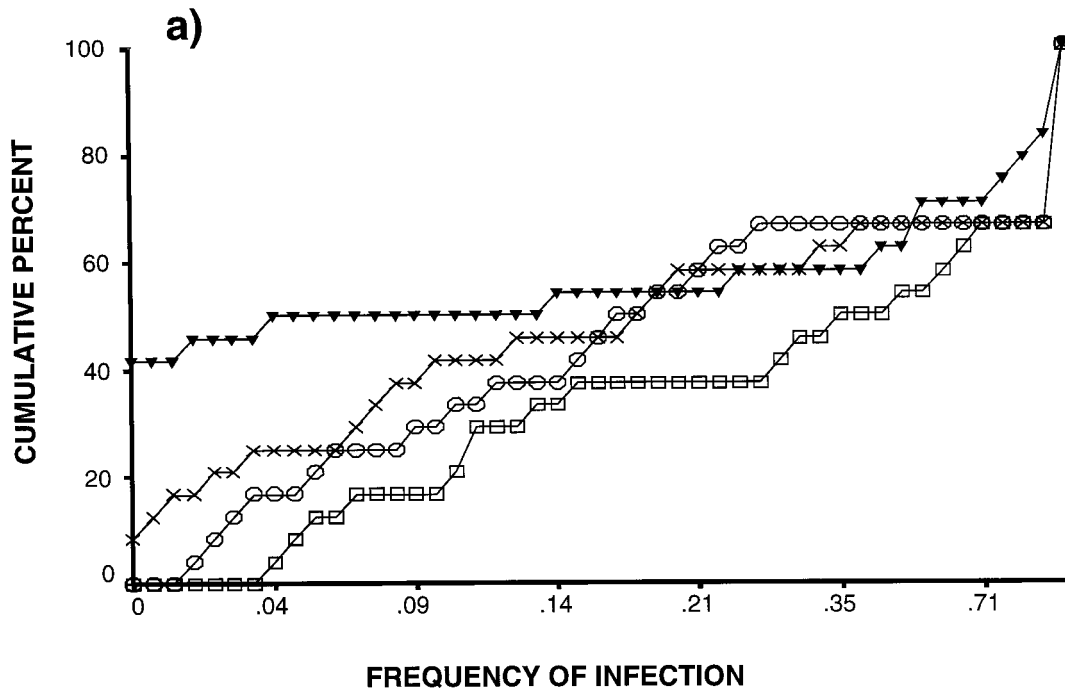


FIG. 6. Cumulative percentage of simulations resulting in infection frequency less than or equal to abscissa value. Infection frequencies refer to the end of simulations ($t = 200$). Host spatial dispersions are agricultural (square), statistically uniform (circle), random (x), and clumped (triangle). Each abscissa is scaled logarithmically to show differences at low infection frequencies. Low frequencies of infection occur least often for agriculturally dispersed hosts. Low frequencies of infection are most common for clumped hosts.

both mean-field and pair approximations. Overall, the mean-field model produced greater levels of infestation than observed in simulation of the spatially detailed model. Mean-field dynamics most closely approximated simulation results for agriculturally arrayed hosts. The mean-field model deviated most from simulations when hosts were clumped, i.e., arrayed most heterogeneously.

For the lower level of α/δ , pair approximations matched the simulations' frequency of infestation better than did the mean-field model. However, the pair approximation often exceeded the level of infestation observed in simulation, especially for clumped hosts. At the greater level of α/δ , the difference between mean-field and pair approximations declined. Each model predicted fairly rapid advance of the vector, often faster than observed in the spatially detailed model.

To compare the levels of infestation in some detail, we consider a case where the vector failed to advance in simulation and then a case where infestation is substantial by the end of simulation. Figures 7a–7c show mean-field dynamics, pair approximation, and simulation results for uniform, random and clumped hosts; both global host density and α/δ are at the lower level. In simulation the vector fails to advance if hosts are randomly arrayed or clumped, and the vector infests only 9% of hosts uniformly dispersed. The mean-field model deviates strongly from the simulations. The three pair approximations clearly do better, but still produce greater levels of infestation than observed in the simulations. Interestingly, the largest difference between pair approximation and simulation occurs when hosts are clumped. Apparently, the limitation host clumping imposes on vector infestation occurs at a spatial scale beyond the neighborhood blocks of pair approximation (Caraco *et al.*, 1998; Ives *et al.*, 1998; Neuhauser, 1998; Hiebeler, 2000).

For a case where the vector advances in simulation, Figs. 8a–8c show mean-field and pair-approximation models along with simulation results. The mean-field and pair approximations have nearly converged in this example; the large neighborhood size and high global density yield model results close to homogeneous mixing. Both approximations exceed the level of infestation observed in simulation; the difference is greatest when hosts are clumped.

To consider infestation and infection simultaneously, we are limited to the mean-field model and simulations. Figure 9a plots mean-field frequencies (x_t/H , y_t/H , and z_t/H) for a parameter combination with low global host density and lower vector-attack probability α . Frequencies of hosts lacking the pathogen and hosts lacking the vector are small (both < 0.06). At $t = 200$, the frequency

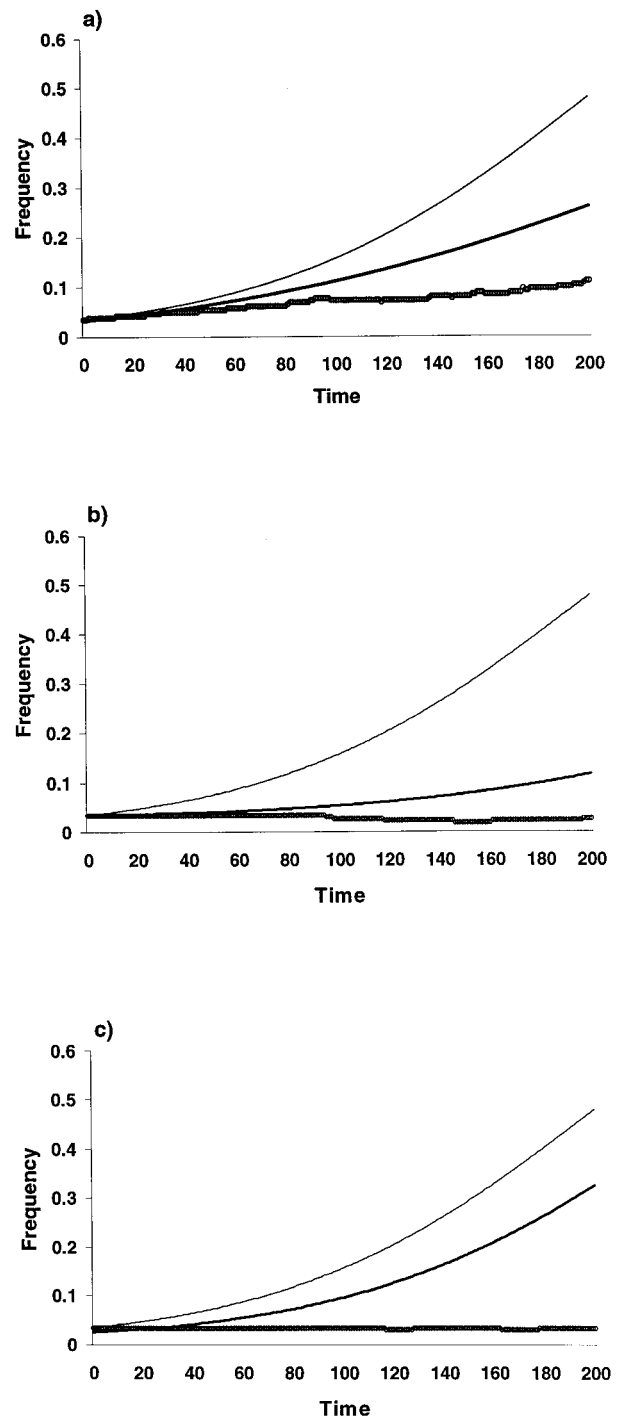


FIG. 7. Vector infestation fails: mean field, pair approximation, and simulation. When the vector fails to advance significantly in simulation, pair approximation better predicts infestation frequencies than does the mean-field model. Simulation parameters are $H = 1/8$, $\delta = 24$, $\alpha = 0.14/\delta$, $\mu = 0.001$. The thinnest line is the mean-field model. The medium line is the pair approximation, and the thickest line is the simulation result. (a) Uniform host array. (b) Random array. (c) Clumped array.

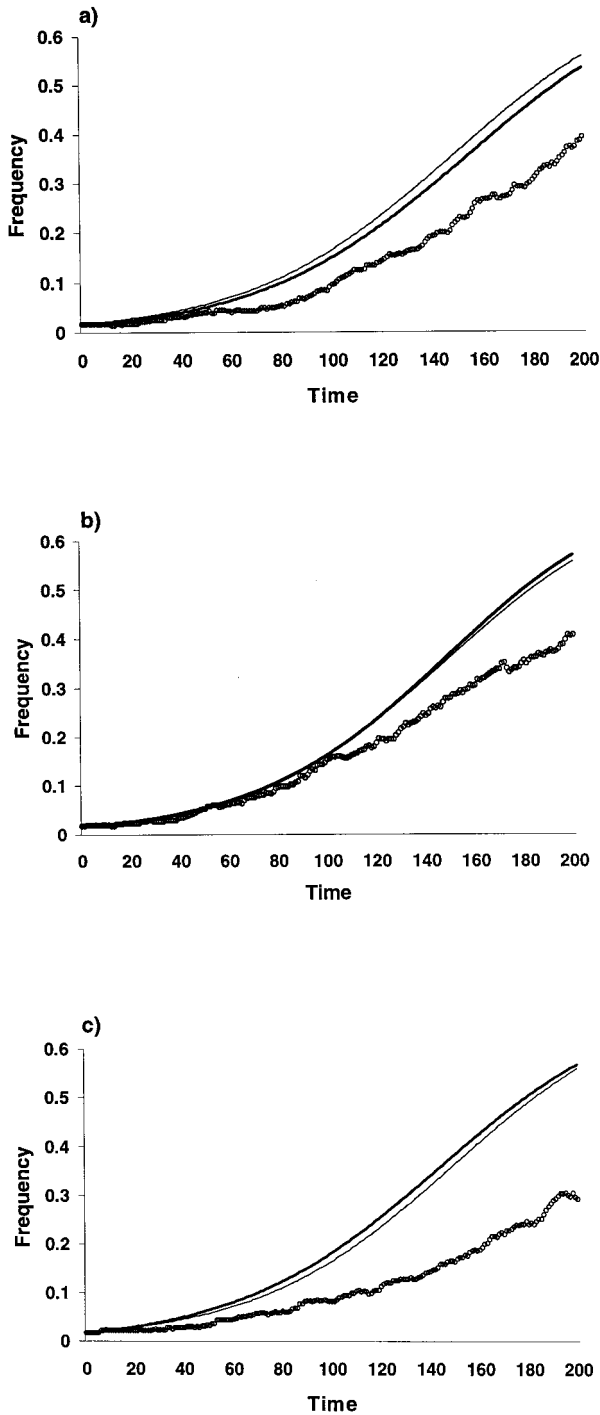


FIG. 8. Vector advances: mean field, pair approximation, and simulation. When the vector advances significantly, mean-field and pair-approximation models behave similarly; both overestimate infestation, especially for clumped hosts. Simulation parameters are $H = 1/4$, $\delta = 224$, $\alpha = 0.14/\delta$, $\mu = 0.01$. The thinnest line is the mean-field model. The medium line is the pair approximation, and the thickest line is simulation result. (a) Uniform host array. (b) Random array. (c) Clumped array.

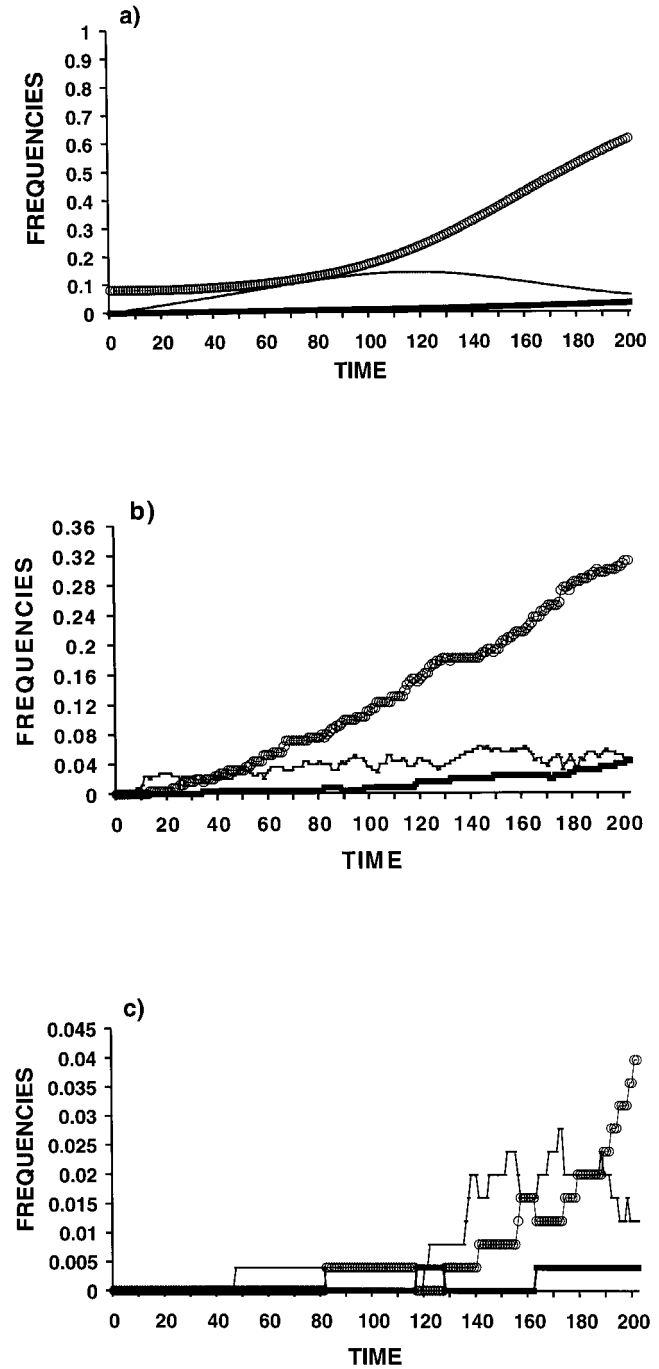


FIG. 9. Comparison of mean-field dynamics and simulations. Ordinates are scaled differently. Parameters are $H = 1/8$, $\alpha = 0.14/\delta$, $\delta = 99$, $\mu = 0.001$, and $\beta = 0.01$. The frequency of hosts infested by the vector, but not infected by the pathogen, is indicated by thin solid line. The frequency of hosts both infested by the vector and infected by the pathogen are indicated by open circles. The frequency of hosts not infested by the vector, but infected by the pathogen, are indicated by a thick solid line. (a) Mean-field dynamics. (b) Spatially detailed simulation, agricultural array. (c) Spatially detailed simulation, clumped hosts.

of hosts both infested and infected (y_{200}/H) is near 0.6. Figure 9b shows the corresponding simulation of the detailed model with hosts arrayed agriculturally, and Fig. 9c shows results for clumped hosts. The frequency of both infestation and infection increases steadily for agricultural hosts, although not as fast as mean-field frequencies. For clumped hosts, most individuals remain free of both vector and pathogen over 200 iterations. Spatial correlations slow the spread of vector-borne

infection, compared to mean-field behavior, and increasing host spatial heterogeneity increases the difference between mean-field and simulation models.

The same parameter values led to the results shown in Fig. 10, but global host density has been increased. For the mean-field dynamics (Fig. 10a), more than 0.9 of the hosts are infested and infected at $t = 200$. For agricultural (Fig. 10b) and clumped (Fig. 10c) hosts, respectively, the corresponding frequencies are near 0.75 and 0.55. Increased host density reduces the difference between results, but effects of spatial heterogeneity remain.

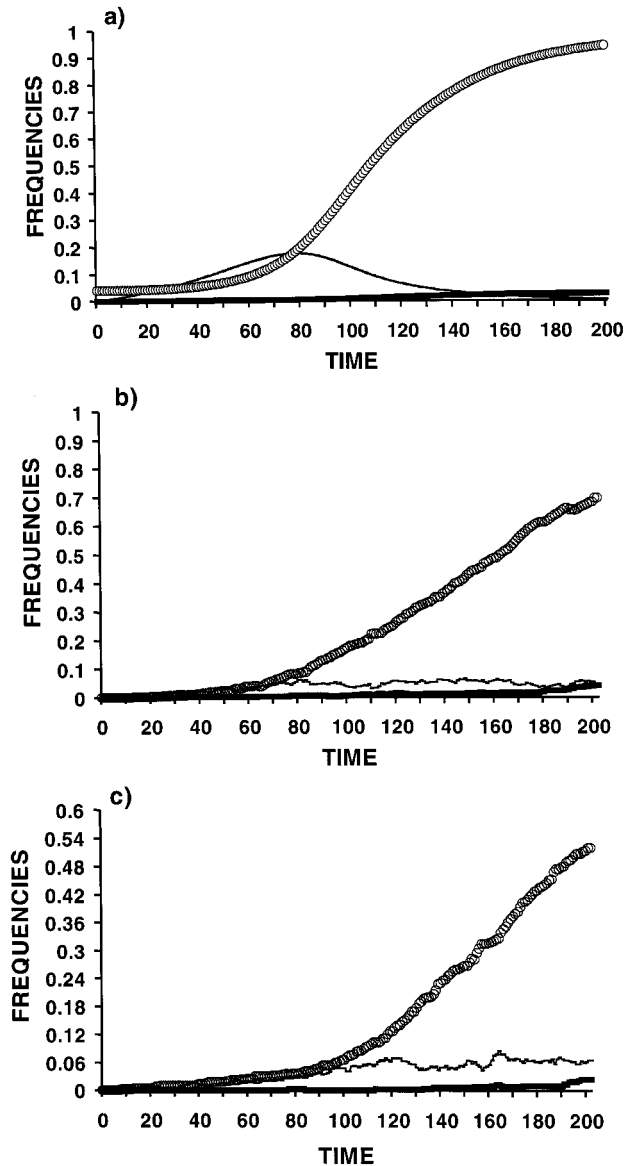


FIG. 10. Comparison of mean-field dynamics and simulations. Ordinates are scaled differently. Parameters are $H = 1/4$, $\alpha = 0.14/\delta$, $\delta = 0.001$, and $\beta = 0.01$. Symbols are as in Fig. 9. (a) Mean-field dynamics. (b) Spatially detailed simulation, agricultural array. (c) Spatially detailed simulation, clumped hosts.

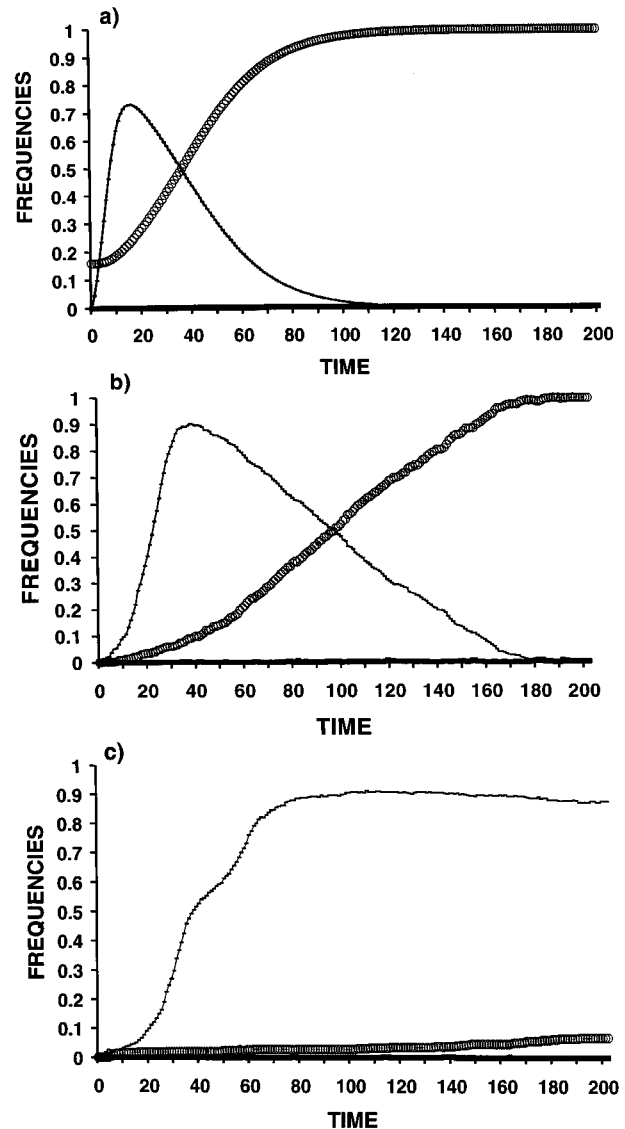


FIG. 11. Comparison of mean-field dynamics and simulations. Parameters are $H = 1/4$, $\alpha = 1/4/\delta$, $\delta = 24$, $\mu = 0.001$, and $\beta = 0.01$. Symbols as in Fig. 9. (a) Mean-field dynamics. (b) Spatially detailed simulation, agricultural array. (c) Spatially detailed simulation, clumped hosts; note the vector-pathogen difference.

Finally, Fig. 11 shows an example, for $\delta = 24$, where the mean-field equations (Fig. 11a) and simulation with agricultural host (Fig. 11b) behave similarly. But the simulation with clumped hosts (Fig. 11c) exhibits vector-pathogen separation. The vector (x_t/H) advances, but the total frequency of infected hosts ($y_t/H + z_t/H$) remains less than 0.1 through the simulation with clumping. Overall, increasing spatial heterogeneity decreases the mean-field model's capacity to approximate the spatial process.

8. DISCUSSION

Our general result suggests that, at the scales of neighborhood size (vector-dispersal distance) and host dispersion studied, increasing host spatial heterogeneity decreases the frequency of vector-borne infection during epidemics of fixed duration. Host spatial heterogeneity can limit spread of the vector, and so constrain the pathogen's prevalence. Furthermore, host spatial heterogeneity can increase the likelihood that vector and pathogen become physically separated, by chance, before many hosts have been infected. The latter effect of host heterogeneity, however, apparently requires smaller neighborhood sizes.

We simulated three neighborhood sizes, since varying neighborhood size yields some important insights about the behavior of spatial models (e.g., Maniatty, *et al.*, 1998). Our results include a strong interaction between neighborhood size and host dispersion. The frequency of infection was particularly low when the vector's advance was inhibited by the combination of small neighborhood size and clumped hosts (Duryea *et al.*, 1999).

Host clumping reduces the vector's spread in two ways. Although clumping may allow a rare vector to remain extant (Bolker, 1999), spatial aggregation of hosts can increase the fraction of vector attacks directed to already infested hosts (Ives *et al.*, 1998). Clumping also generates gaps in the host population, and the requirement for clump-to-clump dispersal can inhibit diffusive spread of the vector (Caraco *et al.*, 1998; Neuhauser, 1998; see Swinton, 1998).

Keeling and Grenfell (1997) analyze a directly transmitted infection where the length of the infectious period varies randomly. That is, the length of time during which an infectious host can transmit the disease to a susceptible host (before recovery or removal) is a continuous random variable. Increasing the variance of the infectious period increases the likelihood that an infective fails to

transmit the disease (Keeling and Grenfell, 1997). In a complementary manner the two models indicate that variability (spatial or temporal) in the rate at which a vector or pathogen advances locally impedes the global advance. Furthermore, heterogeneity among individuals in susceptibility to infestation or infection (α and β in our model) can reduce the frequency of disease in certain epidemic processes (Becker and Marschner, 1990; see Dwyer *et al.*, 1997).

The model's vector attacks uninfested hosts with probability α uniformly across the interaction neighborhood and does not attack outside the neighborhood. Mollison (1972) simulated direct contact infection in one dimension. He compared several patterns of dependence of infection probability on distance from infectious hosts, including uniform distributions (as above) and geometric decay with distance. As long as the maximal distance over which infection could spread was bounded, the epidemic's progress was similar; disease advanced in a steady, wavelike manner (Mollison, 1972). However, at extended spatial scales the chance of long-distance transmission, hence the rate at which a disease spreads, depends on the manner of decay with distance (leptokurtic versus platykurtic distance distributions; Shaw, 1995; Kot *et al.*, 1996; Hart and Gardner, 1997; Lewis, 1997). For a discussion of related points, see Fast and Efimov (1991), Fahrig (1992), or Bevers and Flather (1999).

APPENDIX

The Appendix restricts attention to the mean-field approximation for the spatially detailed model. From the mean-field equations in the text, x_t is the global density of vector-infested and -uninfested hosts, y_t is the global density of infested and pathogen-infested hosts, and z_t is the global density of uninfested and infected hosts. The total density of host individuals, H , is fixed. So, $0 \leq x_t, y_t, z_t \leq H$. At equilibrium, $x_{t+1} = x_t = x^*$, $y_{t+1} = y_t = y^*$, and $z_{t+1} = z_t = z^*$. By definition, vector extinction qualifies as an equilibrium. In this case, $x^* = y^* = 0$; $0 < z^* \leq H$. The dynamics are trapped by vector extinction; no further advance of the pathogen is possible. z^* is simply $z_{t'}$, where t' is the time when the vector goes extinct.

The mean-field equations also admit an infestation-recovery equilibrium. Suppose that the vector persists as time grows large. Since the total number of hosts N is finite, and recovery from the pathogen does not occur, $x^* \rightarrow 0$ as $t \rightarrow \infty$. That is, persistence of the vector on a finite lattice implies that every host eventually

acquires the pathogen. So, at the infestation–recovery equilibrium, we have $x^* = 0$, $0 < y^* < H$, and $0 < z^* < H$; and $y^* + z^* = H$ when the vector persists.

Assuming that the vector persists, the equilibrium frequency of infestation among hosts, y^*/H , satisfies

$$\frac{y^*}{H} = \left[1 + \frac{\mu}{1 - (1 - \alpha y^*)^\delta} \right]^{-1}. \quad (\text{A.1})$$

The associated equilibrium frequency of infected, but uninfested, hosts z^*/H satisfies

$$\frac{z^*}{H} = \left[1 + \frac{1 - (1 - \alpha y^*)^\delta}{\mu} \right]^{-1}. \quad (\text{A.2})$$

All hosts are pathogen-infected when the vector persists. Numerical evaluation of Eq. (A.1) reveals that the equilibrium frequency of vector infestation, y^*/H , increases with both α and neighborhood size δ (Duryea *et al.*, 1999). As the interaction neighborhood and total site number J increase, the frequency of vector infestation approaches $(1 + \mu)^{-1}$.

Vector extinction is always feasible. Existence of the infestation–recovery equilibrium depends on $P(x_t, y_t, z_t)$, the map for the summed total densities of parasitized hosts ($x_t + y_t$); see Eq. (15). Using Eq. (15),

$$\begin{aligned} \Gamma' &= \frac{\partial \Gamma}{\partial (x_t + y_t)} = (1 - \alpha[x_t + y_t]^{\delta-1})(1 - \alpha[x_t + y_t] \\ &\quad + \alpha\delta[H - x_t - y_t]) - \mu. \end{aligned} \quad (\text{A.3})$$

First consider vector extinction, where $x^* = y^* = 0$. The extinction equilibrium is stable if $\Gamma'(x_t = y_t = 0) < 1$, since Γ_t then cannot grow near extinction. Evaluation (A.3) under this condition shows that vector extinction is locally stable and the only mean-field equilibrium, if the expected number of infestations per initial infestation (the vector's basic reproductive rate) is less than unity. However, if $\alpha\delta H/\mu > 1$, $\Gamma'(x_t = y_t = 0) > 1$; pathogen extinction is unstable in the mean-field model, and the infestation–recovery equilibrium is feasible.

Assuming that $\alpha\delta H/\mu > 1$, local stability of the mean-field model's infestation–recovery equilibrium requires

$$|(1 - \alpha y^*)^{\delta-1} (1 - \alpha y^* + \alpha H \delta) - \mu| < 1. \quad (\text{A.4})$$

As $J \rightarrow \infty$, and $\delta \rightarrow J$, $y^*/H \rightarrow (1 + \mu)^{-1}$. The absolute value of Γ' at the infestation–recovery equilibrium approaches μ , so that stability condition (A.4) must be met.

ACKNOWLEDGMENT

We appreciate the support of NSF Grant BIR-9320264. We thank the four reviewers for their very useful comments.

REFERENCES

- Becker, N., and Marschner, I. 1990. The effect of heterogeneity on the spread of disease, in "Stochastic Processes in Epidemic Theory" (J.-P. Gabrile, C. Lefèvre, and P. Picard, Eds.), Lecture Notes in Biomathematics, pp. 90–103, Springer-Verlag, New York.
- Bevers, M., and Flather, C. H. 1999. Numerically exploring habitat fragmentation effects on populations using cell-based coupled map lattices, *Theor. Popul. Biol.* **55**, 61–76.
- Bolker, B. M. 1999. Analytic models for the patchy spread of plant disease, *Bull. Math. Biol.* **61**, 849–874.
- Bolker, B., and Pacala, S. W. 1997. Using moment equations to understand stochastically driven spatial pattern formation in ecological systems, *Theor. Popul. Biol.* **52**, 179–197.
- Bramson, M., Durrett, R., and Swindle, G. 1989. Statistical mechanics of crabgrass, *Ann. Probab.* **17**, 444–481.
- Burdon, J. J., and Chilvers, G. A. 1975. Epidemiology of damping-off disease (*Pythium irregulare*) in relation to density of *Lepidium sativum* seedlings, *Ann. Appl. Biol.* **81**, 135–143.
- Burdon, J. J., Jarosz, A. M., and Kirby, G. C. 1989. Pattern and patchiness in plant–pathogen interactions: Causes and consequences, *An. Rev. Ecol. Syst.* **20**, 119–136.
- Caraco, T., Duryea, M., Gardner, G., Maniatty, W., and Szymanski, B. K. 1998. Spatial heterogeneity and extinction of an SIS epidemic, *J. Theor. Biol.* **192**, 351–361.
- Carter, N., and Harrington, R. 1991. Factors influencing aphid population dynamics and behavior and the consequences for virus spread, in "Advances in Disease Vector Research, Volume 7" (K. F. Harris, Ed.), pp. 19–51, New York.
- Claessen, D., and de Roos, A. M. 1995. Evolution of virulence in a host–pathogen system with local pathogen transmission, *Oikos* **74**, 401–413.
- Cohen, J. E. 1971. "Casual Groups of Monkeys and Men," Harvard Univ. Press, Cambridge, MA.
- Diggle, P. 1983. "Statistical Analysis of Spatial Point Patterns," Academic Press, New York.
- Durrett, R., and Levin, S. A. 1994. Stochastic spatial models: A user's guide to ecological applications, *Phil. Trans. R. Soc. London, Ser. B* **343**, 329–350.
- Duryea, M., Caraco, T., Gardner, G., Maniatty, W., and Szymanski, B. K. 1999. Population dispersion and equilibrium infection frequency in a spatial epidemic, *Phys. D* **132**, 511–519.
- Dwyer, G. 1992. On the spatial spread of insect viruses: theory and experiment, *Ecology* **73**, 479–494.
- Dwyer, G., and Elkinton, J. S. 1995. Host dispersal and the spatial spread of insect populations, *Ecology* **76**, 1262–1275.
- Dwyer, G., Elkinton, J. S., and Buonaccorsi, J. P. 1997. Host heterogeneity in susceptibility and disease dynamics: Tests of a mathematical model, *Am. Nat.* **150**, 685–707.
- Ellner, S. P., Sasaki, A., Haraguchi, Y., and Matsuda, H. 1998. Speed of invasion in lattice population models: Pair-edge approximation, *J. Math. Biol.* **36**, 469–484.
- Fahrig, L. 1992. Relative importance of spatial and temporal scales in a patchy environment, *Theor. Popul. Biol.* **41**, 300–314.
- Fast, V. G., and Efimov, I. R. 1991. Stability of vortex rotation in an excitable cellular medium, *Phys. D* **49**, 75–81.

- Feller, W. 1957. "An Introduction to Probability Theory and its Applications, Vol. 1, 2nd Ed.," Wiley, New York.
- Gerhardt, M., Schuster, H., and Tyson, J. J. 1990. A cellular automaton of excitable media including curvature and dispersion, *Science* **247**, 1563–1566.
- Greig-Smith, P. 1979. Pattern in vegetation, *J. Ecol.* **67**, 755–779.
- Harada, Y., Ezoe, H., Iwasa, Y., Matsuda, H., and Sato, K. 1995. Population persistence and spatially limited social interaction, *Theor. Popul. Biol.* **48**, 65–91.
- Hart, D. R., and Gardner, R. H. 1997. A spatial model for the spread of invading organisms subject to competition, *J. Math. Biol.* **35**, 939–948.
- Hays, W. L. 1994. "Statistics, Fifth Ed.," Harcourt Brace, Fort Worth, TX.
- Hiebeler, D., 1997. Stochastic spatial models: From simulations to mean field and local structure approximations, *J. Theor. Biol.* **187**, 307–319.
- Hiebeler, D. 2000. Populations on fragmented landscapes with spatially structured heterogeneities: Landscape generation and local dispersal, *Ecology* **81**, 1629–1641.
- Holmes, E. E., 1997. Basic epidemiological concepts in a spatial context, in "Spatial Ecology" (D. Tilman and P. Kareiva, Eds.), pp. 111–136, Princeton Univ. Press, Princeton, NJ.
- Ives, A. R., Turner, M. G., and Pearson, S. M. 1998. Local explanations of landscape patterns: Can analytical approaches approximate simulation models of spatial processes?, *Ecosystems* **1**, 35–51.
- Kareiva, P. 1990. Population dynamics in spatially complex environments: Theory and data, *Phil. Trans. R. Soc. London Ser. B* **330**, 175–190.
- Keeling, M. J., and Grenfell, B. T. 1997. Disease extinction and community size, *Science* **275**, 65–67.
- Kot, M., Lewis, M. A., and van den Driessche, P. 1996. Dispersal data and the spread of invading organisms, *Ecology* **77**, 2027–2042.
- Law, R., and Dieckmann, U. 2000. A dynamical system for neighborhoods in plant communities, *Ecology* **81**, 2137–2148.
- Levin, S. A., Grenfell, B., Hastings, A., and Perelson, A. S. 1997. Mathematical and computational challenges in population biology and ecosystems science, *Science* **275**, 334–343.
- Lewis, M. A., 1997. Variability, patchiness and jump dispersal in the spread of an invading population, in "Spatial Ecology" (D. Tilman and P. Kareiva, Eds.), pp. 46–69, Princeton Univ. Press, Princeton, NJ.
- Maniatty, W., Szymanski, B., and Caraco, T. 1994. Implementation and performance of parallel ecological simulations, in "Applications in Parallel and Distributed Computing" (C. Girault, Ed.), pp. 93–102, North-Holland, Amsterdam, The Netherlands.
- Maniatty, W. A., Szymanski, B. K., and Caraco, T. 1998. Parallel computing with generalized cellular automata, *Paral. Distr. Comp. Pract.* **1**, 31–50.
- Matsuda, H., Ogita, N., Sasaki, A., and Sato, K. 1992. Statistical mechanics of population, *Prog. Theor. Phys.* **88**, 1035–1049.
- McElhany, P., Real, L. A., and Power, A. G. 1995. Vector preference and disease dynamics: A study of barley yellow dwarf virus, *Ecology* **76**, 444–457.
- Mollison, D. 1972. The rate of spatial propagation of simple epidemics, *Proc. Sixth Berkeley Symp. Math. Stat. Prob.* **3**, 579–614.
- Mollison, D. 1977. Spatial contact models for ecological and epidemic spread, *J. R. Stat. Soc. Ser. B* **39**, 283–326.
- Mollison, D., and Kuulasmaa, K. 1985. Spatial epidemic models: Theory and simulation, in "Population Dynamics of Rabies in Wildlife" (P. J. Bacon, Ed.), pp. 291–309, Academic Press, London.
- Nakamura, M., Matsuda, H., and Iwasa, Y. 1997. The evolution of cooperation in a lattice-structured population, *J. Theor. Biol.* **184**, 65–81.
- Neuhauser, C. 1998. Habitat destruction and competitive coexistence in spatially explicit models with local interactions, *J. Theor. Biol.* **193**, 445–463.
- Onstad, D. W., Maddox, J. V., Cox, D. J., and Kornkven, E. A. 1990. Spatial and temporal dynamics of animals and the host-density threshold in epizootiology, *J. Invert. Path.* **55**, 76–84.
- Rand, D. A., Keeling, M., and Wilson, H. B. 1995. Invasion, stability and evolution to criticality in spatially extended, artificial host-pathogen ecologies, *Proc. R. Soc. London Ser. B* **259**, 55–63.
- Real, L. A., and McElhany, P. 1996. Spatial pattern and process in plant–pathogen interactions, *Ecology* **77**, 1011–1025.
- Rhodes, C. J., and Anderson, R. M. 1996. Persistence and dynamics in lattice models of epidemic spread, *J. Theor. Biol.* **180**, 125–133.
- Sato, K., Matsuda, H., and Sasaki, A. 1994. Pathogen invasion and host extinction in lattice structures populations, *J. Math. Biol.* **32**, 251–268.
- Shaw, M. W. 1995. Simulation of population expansion and spatial pattern when individual dispersal distributions do not decline exponentially with distance, *Proc. R. Soc. B* **259**, 243–248.
- Swinton, J. 1998. Extinction times and phase transitions for spatially structured closed epidemics, *Bull. Math. Biol.* **60**, 215–230.
- Swinton, J., and Anderson, R. M. 1995. Model frameworks for plant–pathogen interactions, in "Ecology of Infectious Diseases in Natural Populations" (B. T. Grenfell and A. P. Dobson, Eds.), pp. 280–294, Cambridge Univ. Press, Cambridge, UK.
- Szymanski, B., and Caraco, T. 1994. Spatial analysis of vector-borne disease: A four-species model, *Evol. Ecol.* **8**, 299–314.
- Wilbur, W. J., Lipman, D. J., and Shamma, S. A. 1986. On the prediction of local patterns in cellular automata, *Phys.* **19**, 397–410.